AD-A079 516 CALIFORNIA UNIV LOS ANGELES DEPT OF ELECTRICAL SCIEN--ETC F/G 20/9
WAVES AND INSTABILITIES IN STEADY-STATE HIGH-BETA PLASMAS.(U)
OCT 79 N C LUHMANN, F F CHEN F49620-76-C-0012
UNCLASSIFIED UCLA-ENG-7964 AFOSR-TR-79-1312 NL

| OF |
AD A079 516

END
DATE FILMED
2-80
DDC

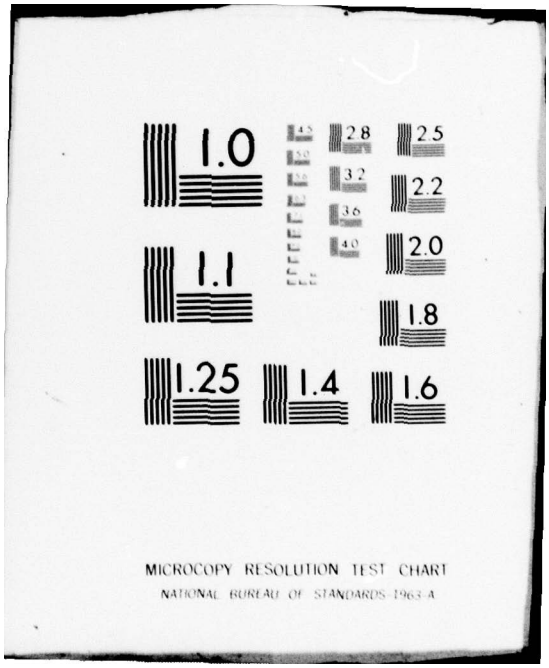
1.0
1.1
1.25
1.4
1.6
2.8
3.2
3.6
4.0
2.5
2.2
2.0
1.8
MICROCOPY RESOLUTION TEST CHART
NATIONAL BUREAU OF STANDARDS-1963-A

UCLA SCHOOL OF ENGINEERING AND APPLIED SCIENCE

ANNUAL SCIENTIFIC REPORT

LEVEL II

Research sponsored by the
Air Force Office of Scientific Research
Air Force Systems Command, USAF,
under Contract No. F49620-76-C-0012

Contract Period: October 1, 1978 to September 30, 1979

WAVES AND INSTABILITIES IN STEADY-STATE HIGH-BETA PLASMAS

UCLA-ENG. 7964
OCTOBER 1979

Principal Investigator: N. C. Luhmann Jr.
Associate Professor

Co-Principal Investigator: F. F. Chen
Professor

UCLA • SCHOOL OF ENGINEERING AND APPLIED SCIENCE

UNCLASSIFIED

SECURITY CLASSIFICATION OF THIS PAGE (When Data Entered)

(19) REPORT DOCUMENTATION PAGE

READ INSTRUCTIONS BEFORE COMPLETING FORM

(18) AFOSR-TR--79-1312

2. GOVT ACCESSION NO.

3. RECIPIENT'S CATALOG NUMBER

4. TITLE (and Subtitle)

(6) WAVES AND INSTABILITIES IN STEADY-STATE HIGH-BETA PLASMAS,

5. TYPE OF REPORT & PERIOD COVERED
Annual Report
Oct. 1, 1978 to Sept. 30, 1979

6. PERFORMING ORG. REPORT NUMBER
ENG-7964

7. AUTHOR(s)

(10) N. C. Luhmann, Jr. & Frances F. Chen

8. CONTRACT OR GRANT NUMBER(s)

(15) F49620-76-C-0012

9. PERFORMING ORGANIZATION NAME AND ADDRESS

Department of Electrical Sciences
7731 Boelter Hall, University of California
Los Angeles, California 90024

10. PROGRAM ELEMENT, PROJECT, TASK AREA & WORK UNIT NUMBERS
61102F 2301/A7

11. CONTROLLING OFFICE NAME AND ADDRESS

Air Force Office of Scientific Research/NP
Bolling Air Force Base, Bldg. #410
Wash DC 20332

(11) 12. REPORT DATE
October 1979

13. NUMBER OF PAGES
81

(12) 85

14. MONITORING AGENCY NAME & ADDRESS(if different from Controlling Office)

(9) Annual rept. 1 Oct 78 - 30 Sep 79,

15. SECURITY CLASS. (of this report)
Unclassified

15a. DECLASSIFICATION/DOWNGRADING SCHEDULE

16. DISTRIBUTION STATEMENT (of this Report)

Approved for public release; distribution unlimited

(16) 2301

(17) A7

17. DISTRIBUTION STATEMENT (of the abstract entered in Block 20, if different from Report)

(14) UCLA-ENG-7964

18. SUPPLEMENTARY NOTES

19. KEY WORDS (Continue on reverse side if necessary and identify by block number)
Microwave Experimental Simulations of Laser-Plasma Interactions
Spontaneous Magnetic Field Generation
Profile Modifications
Resonance Absorption and Parametric Instability
Soliton Flash
Finite Beta Waves and Instabilities
Steady-State, High Density, Fully-Ionized Plasma Sources

20. ABSTRACT (Continue on reverse side if necessary and identify by block number)

Stimulated Brillouin scattering has been conclusively identified in a microwave simulation experiment. The threshold and initial growth rate are in agreement with the convective finite interaction length theory. Saturation of the SBS ion waves and associated backscattered electromagnetic wave are observed and a tentative identification of ion trapping as the saturation mechanism has been made. Observations of spontaneous magnetic field generation at low power continued in an attempt to conclusively identify the saturation mechanism. The soliton flash has been studied together with the associated

DD FORM 1 JAN 73 1473 EDITION OF 1 NOV 65 IS OBSOLETE 409 432 UNCLASSIFIED JOB

phenomena such as hot electron production, spontaneous magnetic field generation and ion wave instabilities. The finite beta waves and instabilities effort has also continued with primary emphasis on large diameter, high density plasma production.

Unclassified

UCLA- ENG. 7964
OCTOBER 1979

ANNUAL SCIENTIFIC REPORT

WAVES AND INSTABILITIES IN STEADY-STATE HIGH-BETA PLASMAS

PRINCIPAL INVESTIGATOR: N. C. Luhmann, Jr.
Associate Professor

CO-PRINCIPAL INVESTIGATOR: Francis F. Chen
Professor

Research sponsored by the
Air Force Office of Scientific Research
Air Force Systems Command, USAF,
under Contract No. F49620-76-C-0012

Contract Period: October 1, 1978 to September 30, 1979

Electrical Sciences and Engineering Department
School of Engineering and Applied Science
University of California
Los Angeles, California 90024

TABLE OF CONTENTS

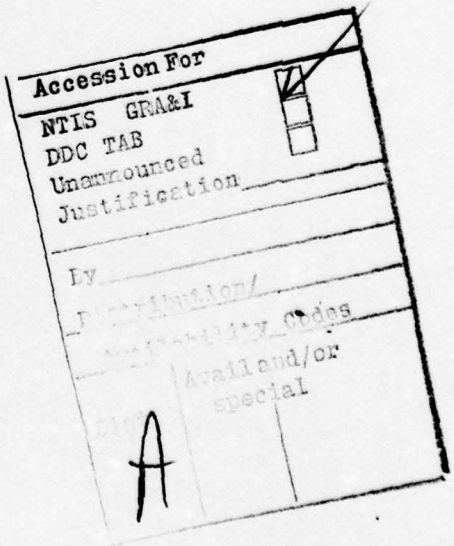

I. INTRODUCTION

The AFOSR funded UCLA Plasma Engineering Laboratory program has continued to concentrate on the physics of laser-plasma interactions and high beta waves and instabilities relevant to the magnetosphere. Specifically the current areas of research include:

1. The study of the physics associated with the use of high power lasers to heat both critical density plasmas (pellets and dense plasma focus) and underdense plasmas (long solenoid). In these studies the wavelenths are scaled from the 1-10 μm region to ≃ 1-10 cm so that large diameter (1-3m) well-diagnosed laboratory plasmas may be employed. In addition, by operating in the 1-10 cm wavelength region, advantage can be taken of the readily available military radar sets. The typical power levels of 0.1-10 MW result in $E_o^2/8\pi KT_e \geq 1$.

2. Continued effort on the development of the lanthanum hexaborhide hollow cathode source as a means of producing large diameter, finite-beta plasma device.

3. Development of new plasma diagnostic systems such as the boxcar data processor described in Sec. IID.

Our progress over the past year is covered in Sec. II. The program on microwave experimental simulations of laser-plasma interactions is covered in Sec. IIA. Our work on stimulated Brillouin-scattering discussed in Sec. IIA has resulted in the first identification of the existence of this phenomenon in a laboratory plasma. This work has been submitted for publication in Physical Review Letters. Spontaneous magnetic field generation due to resonance absorption continued to be the subject of an intensive study as also described in Sec. IIA. Preliminary results were published in Physical Review Letters. To extend our microwave-plasma interaction investigations to higher intensity, two S-band radar transmitters were located on government excess property lists (see Sec. IIB). Both of them are now operational with the lower power ($P \simeq 160$ kW) MORT transmitter used in the magnetic field generation experiments and the higher power ($P \simeq 2$ MW) AWACS unit employed for SBS studies.

There has also been considerable work done on the so-called soliton flash (see Sec. IIA) and associated phenomena. Here the electric field produced by an obliquely incident electromagnetic wave grows to large amplitude near the critical layer and suddenly decreases at $\omega_{pi}\,\tau \simeq 20$. We have verified the theoretical predictions concerning the flash electric field and have demonstrated the dependence of hot electron production, quasi-static magnetic field generation and ion wave instabilities on the flash. This work has been submitted to Physical Review Letters.

Much of the success of our program can be credited to the development of specialized diagnostic equipment which permits the detailed measurement of plasma parameters in our microwave experiments. A survey of the diagnostic development work carried out during the past year is contained in Sec. IID.

A list of publications, presentations and reports completed during the past year are given in Sec. III. The major research personnel are listed in Sec. IV. It should be noted that our program was greatly aided by such visitors as Professor Kawaguchi and Mr. Goebel who had their own financial support.

II. PROGRESS (October 1, 1978 - September 30, 1979)

A. Microwave Experimental Simulations of Laser Plasma Interactions

There is currently considerable interest in laser plasma interactions. Much of this interest is due to the potential applications of CO_2 laser heated dense plasma focus plasmas, CO_2 laser heated long solenoids and CO_2 laser pellet implosions for X-ray sources. Unfortunately, due to the difficulty in making plasma measurements, a detailed understanding of the laser energy absorption mechanisms has not yet emerged. Our approach to understanding these interactions is to scale the phenomena so that microwave sources and well diagnosed low density laboratory plasmas may be employed. During the past year we have been primarily concerned with the study of stimulated Brillouin scattering in the underdense plasma regions ($n \simeq 0.1\ n_{cr}$) and with the study of

spontaneous magnetic field generation due to resonance absorption in addition to the soliton flash.

1. Stimulated Brillouin Scattering

In laser plasma interactions such as CO_2 laser heating of dense plasma focus plasmas, CO_2 heating of long solenoids and CO_2 and Nd-laser-pellet interactions it is important to understand the absorption of laser light. Stimulated Brillouin scattering (SBS)[1-6] is one of the major obstacles for effective absorption of the incident laser light. Recently, in experiments aimed at a more close approximation of actual pellet implosions, SBS has been investigated by using a shaped pulse[5] which has a prepulse forming a long scale length low density plasma and also with a long pulse width and large focal spot[6] laser. Measurements showed greatly enhanced direct backscatter, which exhibits the properties of SBS, and which appeared to originate in an underdense region of the plasma ($n_o < 0.1\ n_{cr}$)[5].

During the past year we have made the first experimental observation of SBS in a microwave interaction with a laboratory unmagnetized plasma. Using such a well-controlled plasma device the threshold power, growth rate and saturation of the instability are easily made. A paper describing these results has been submitted to Physical Review Letters, a copy of which is included in Appendix I. We will therefore only briefly summarize the results in this section.

The experiments are performed in a large unmagnetized plasma (75 cm diameter, 200 cm length) shown in Fig. 1. Microwave radiation

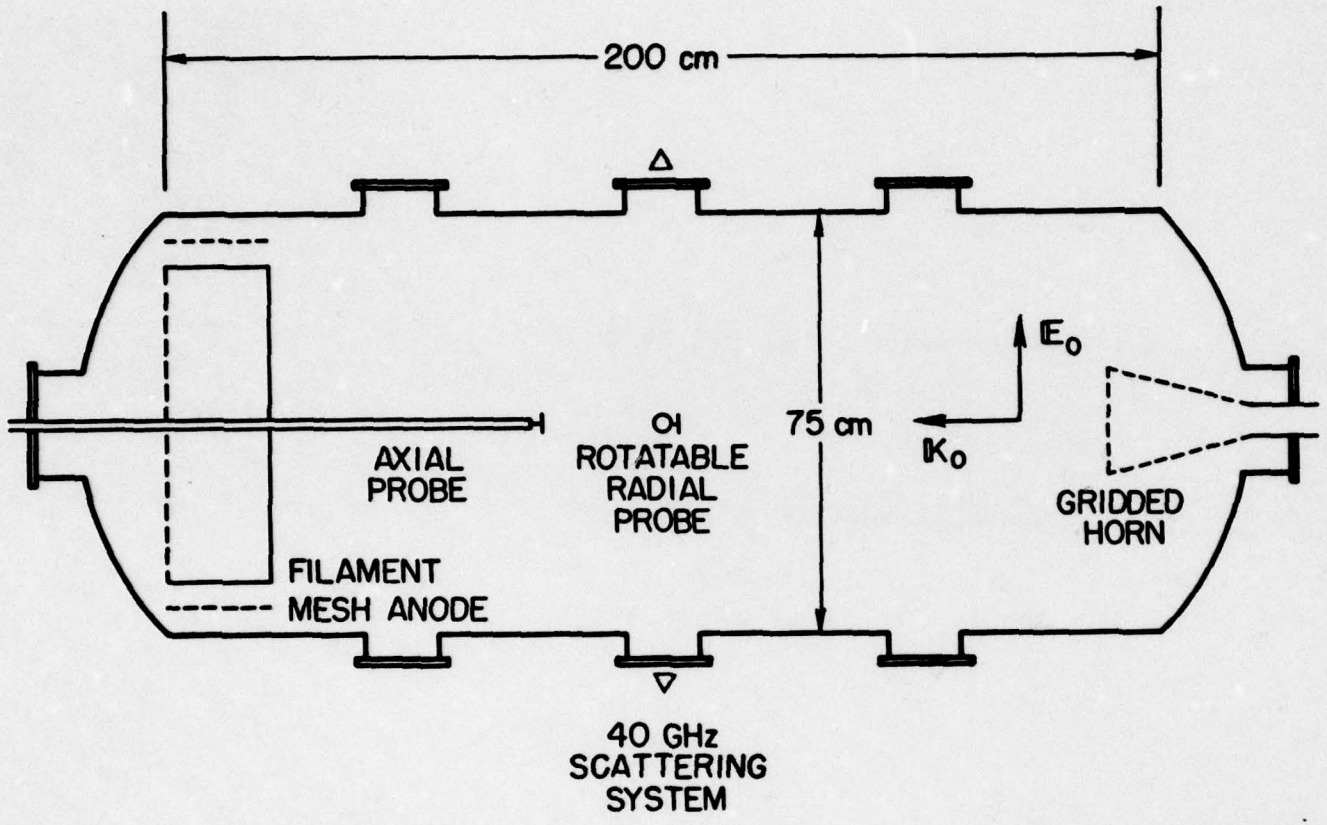

Fig. 1. Apparatus for Microwave Experimental Study of Stimulated Brillouin Scattering.

($\lambda_o \simeq 1.5$-10 cm, $P \leq 1$ MW) is launched along the axis using a gridded horn. The backscattered microwave radiation is monitored so that both the reflectivity and frequency shift are known. Likewise, the ion wave frequency, wavelength and amplitude are also monitored. Our initial experiments were concerned with demonstrating conclusively that SBS could be observed in a microwave simulation experiment. Therefore, we operated at $n \simeq 0.1\, n_{cr}$ to prevent other processes from obscuring the SBS phenomena. We were extremely successful and specifically demonstrated the following:

(a) Energy and Momentum Selection Rules were Satisfied.

(b) Quantitative Agreement with the Finite Interaction-Length Convective Threshold.

(c) Saturation ($\tilde{n}/n_o \simeq 4\%$, $r \simeq 13\%$).

The saturation appeared to be due to ion wave trapping. Typical density fluctuation and reflected power data are shown in Figs. 2, 3 and 4.

More recently, we have initiated experiments on finite bandwidth control of SBS using the AWACS S-band radar described in Sec. IIB.

2. Spontaneous Magnetic Field Generation.

Our smaller plasma device (60 cm diameter, 80 cm long) shown in Fig. 5 is employed exclusively for the study of phenomena which occur in the vicinity of the critical layer. During the past year we have particularly concentrated on determining the mechanism responsible for limiting the quasi-static magnetic fields produced by resonance absorption at low pump intensities ($v_o/v_{te} < 0.04$, $\eta_o = E^2/8\pi nkT_e < 6.5 \times 10^{-4}$).

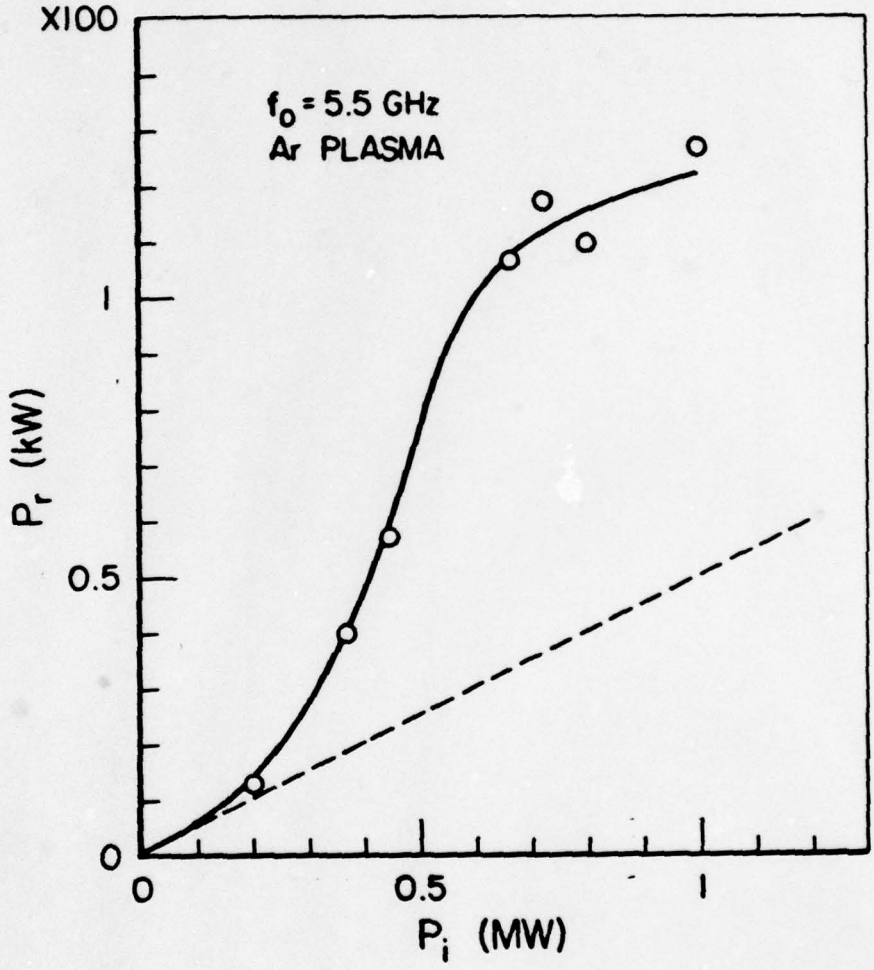

Fig. 2. Total Reflected Power P_r versus Incident Power. The dotted line represents the chamber reflectivity.

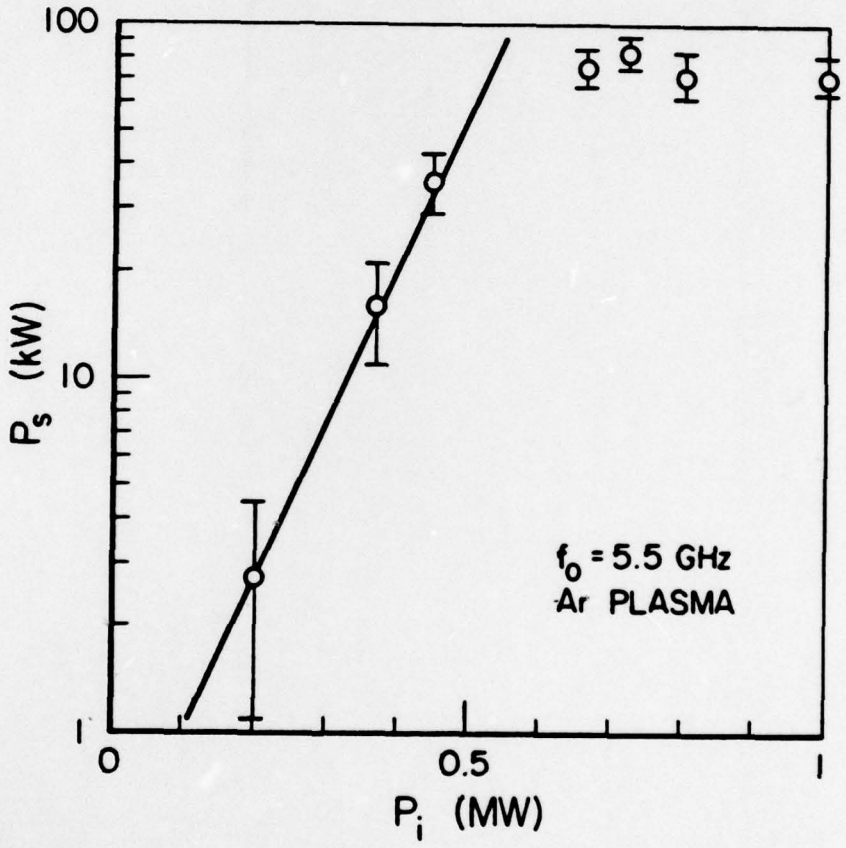

Fig. 3. Scattered Power P_s versus Incident Power P_i. The chamber reflection has been subtracted.

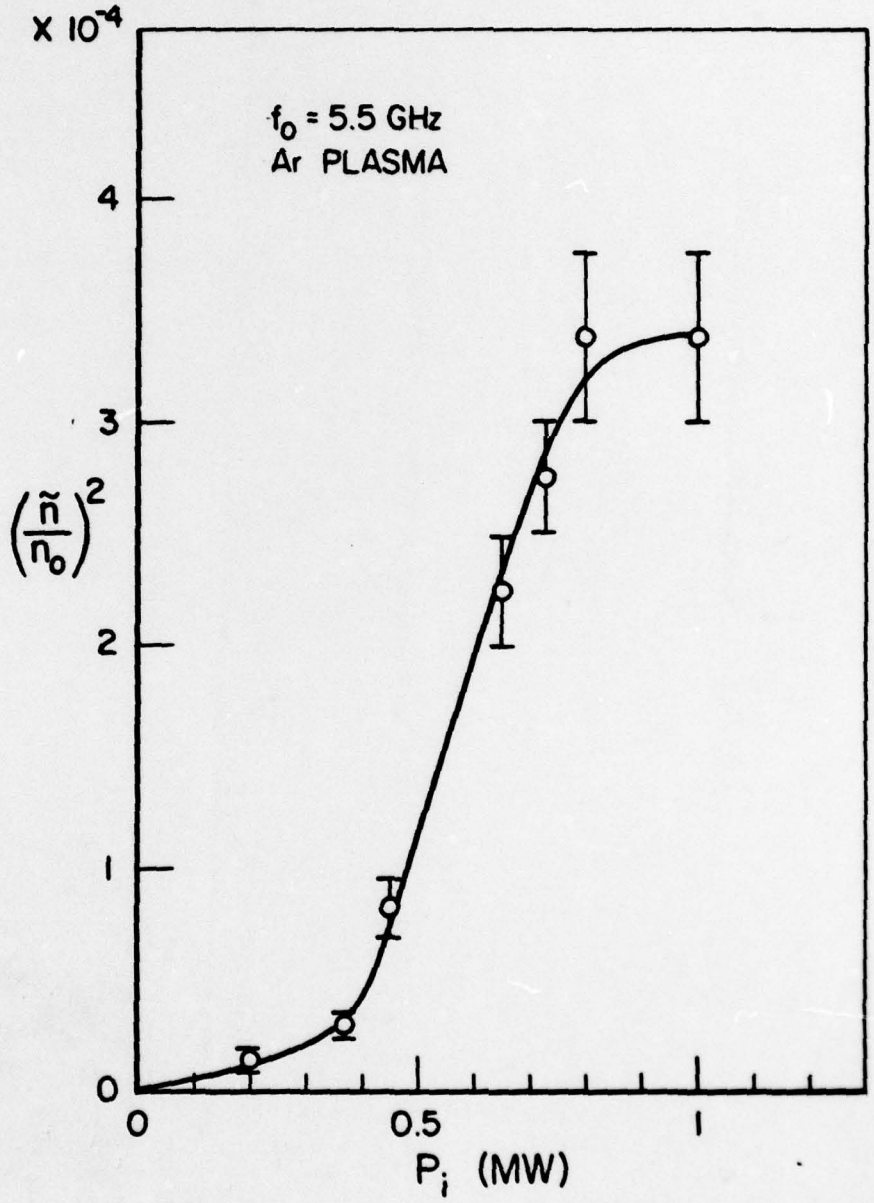

Fig. 4. Normalized Density Fluctuation Amplitude versus Incident Power.

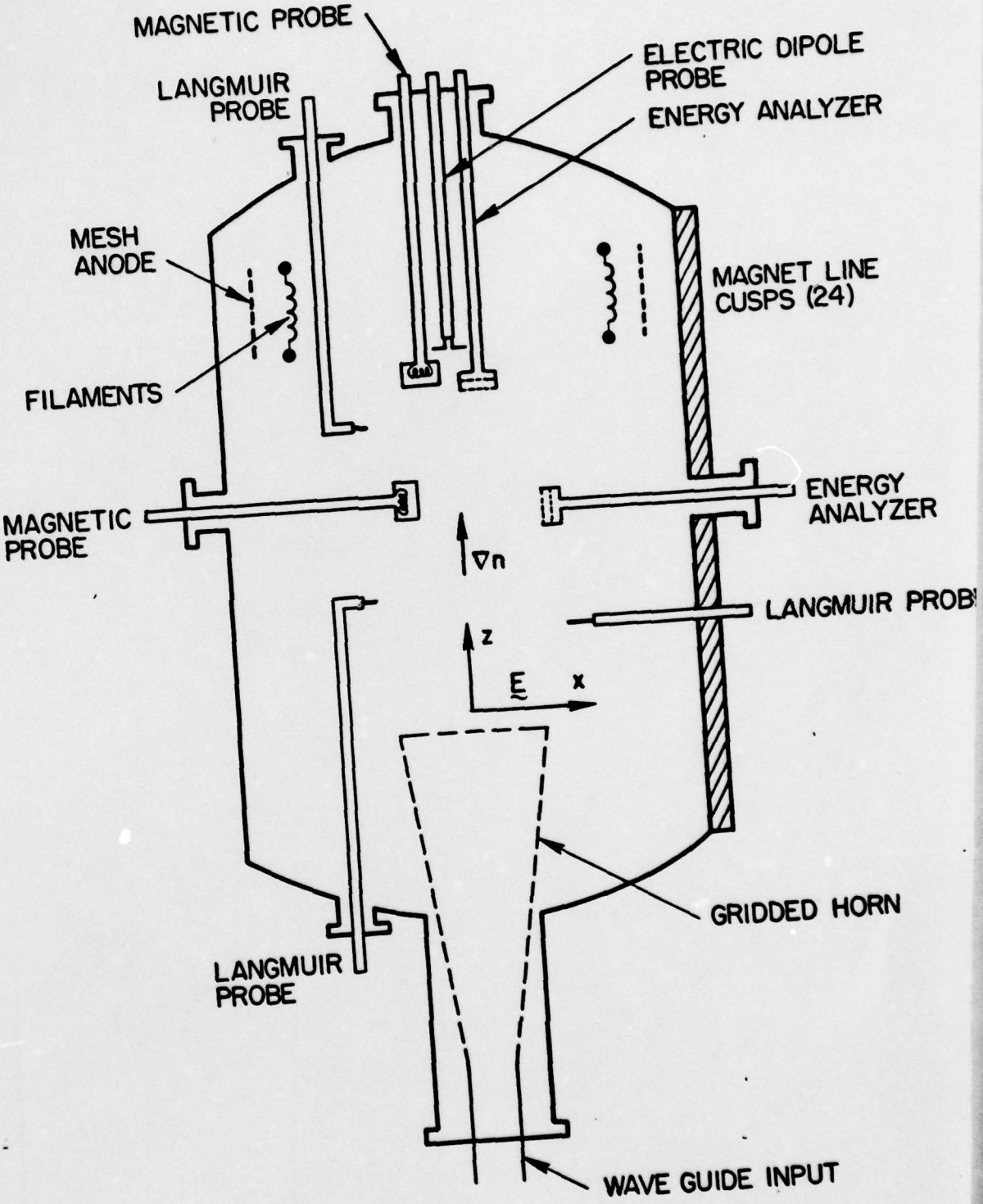

Fig. 5. Experimental Arrangement for the Study of Spontaneous Magnetic Field Generation.

The quasi-static magnetic fields generated by the interaction of microwave radiation with our inhomogeneous plasma are studied using shielded, movable pick-up loops. For the geometry shown in Fig. 5, one expects that the B_y component of the magnetic field should dominate if resonance absorption is the principal field generation mechanism. This is indeed observed with $B_y \geq B_x$ and $B_y > B_z$. In addition, a current sheet of thickness $\simeq$ 5 cm is observed to flow along the incident electric field direction. The initial growth rate of the magnetic field has been measured and found to be constant in time (i.e., $B_y \propto t$) for power levels below approximately 50 W, as expected for resonance absorption. In addition, the absolute value of the measured growth rate (3×10^{-4} G/μs at 80 W) is in good agreement with that predicted by Speziale and Catto[7] (1×10^{-4} G/μs) for resonance absorption generated magnetic fields. The magnetic probe was located approximately 10 cm from the critical layer for these measurements in the overdense plasma region. The magnetic field growth-rate was also studied as a function of incident power for power levels up to 1 kW. As shown in Fig. 6 the growth rate scales linearly with input power up to 50 W and then exhibits a transition to a more nearly $p^{3/2}$ dependence. We note that the former dependence is rigorously maintained while the latter sometimes becomes as rapid as $p^{1.75}$ or even nearly p^2. The p^1 dependence we note is the predicted variation for resonance absorption. The saturated value of B_y was also measured

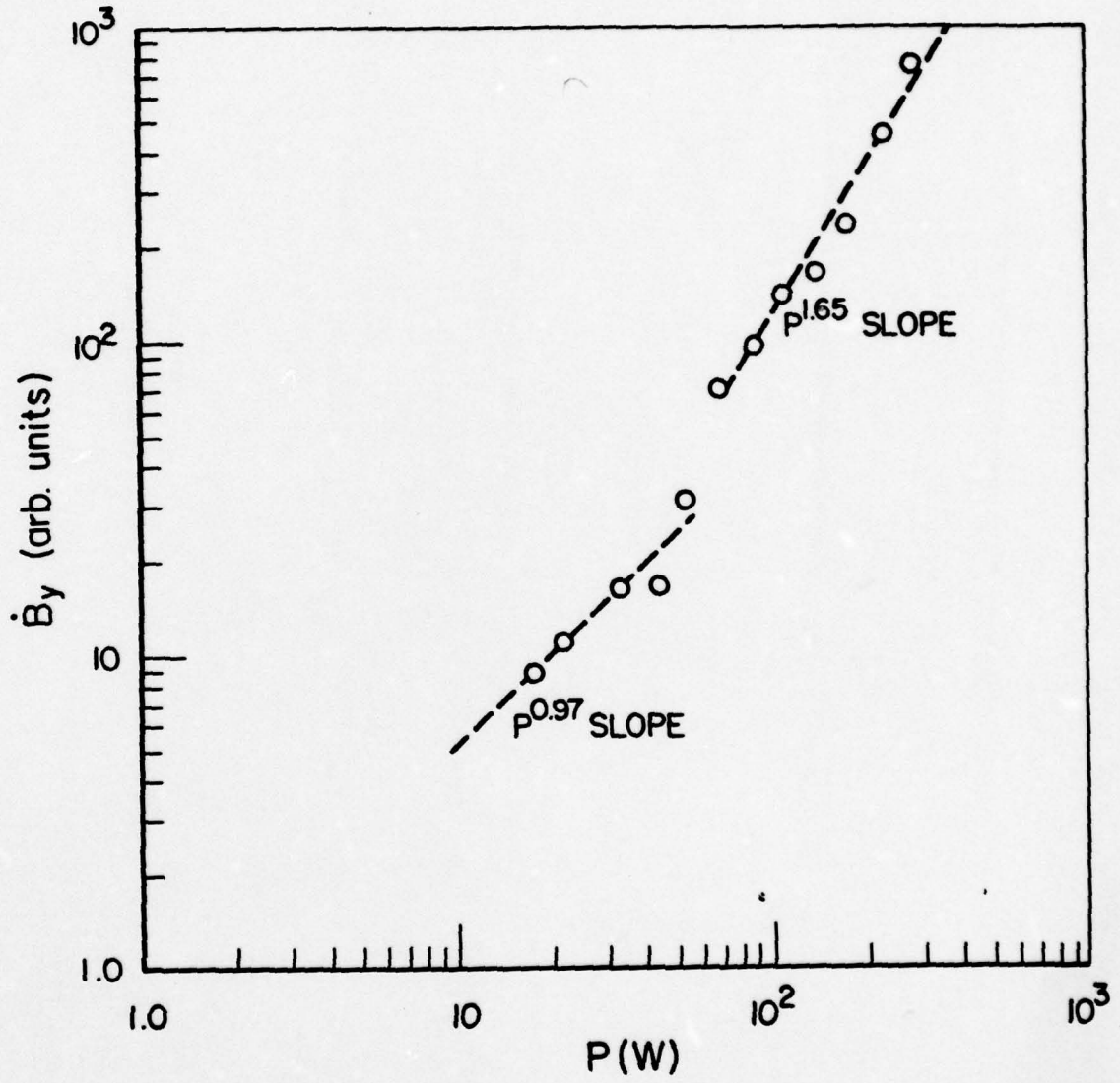

Fig. 6. Growth Rate of Self-Generated Magnetic Field Versus RF Power.

(see Fig. 7) as a function of incident microwave power and was found to exhibit an identical power law dependence to that observed for $\dot{B}_y$. The p^1 dependence for $B_{y,sat}$ is expected as plasma wave convective losses should provide the principal saturation mechanism for these low field intensities. However, we find that the magnitude of the saturated magnetic field is approximately 100 times larger than that predicted by Speziale and Catto[7]. Looking somewhat more closely at our experiment we see that the measured saturation time (.7 μs) is approximately 10 times the thermal convection time given by $(\omega_o L/v_{te})^{2/3}$ which yields $t_c \simeq 70$ nsec for our parameters. It therefore appears that the plasma wave convective losses are being inhibited. A possible mechanism is simply wave trapping in density profile modifications produced by the incident rf.

We therefore first performed measurements with a Langmuir probe to demonstrate the formation of a density cavity near the critical layer even at these low input power levels (< 50 W). The perturbed density profile is shown in Fig. 8 for various times after cessation of a 1 μs duration rf pulse. To demonstrate that these are in fact density changes complete probe I-V characteristic curves were taken with the probe located within the cavity. It was discovered that as expected only the probe electron saturation current had changed and not the slope (electron temperature) or plasma potential. This indicates that the modification of the Langmuir probe signal is due to a

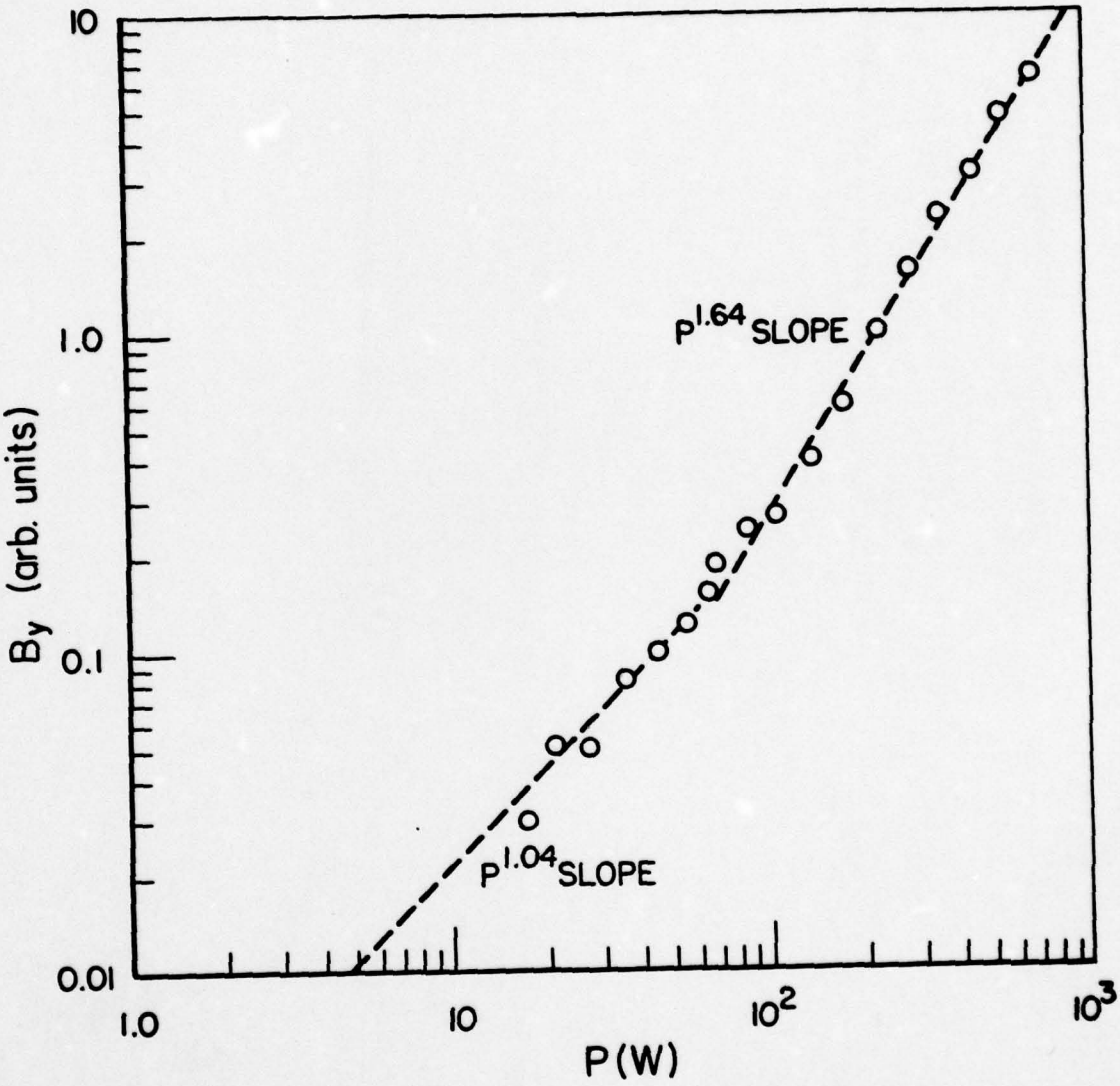

Fig. 7. Saturated Value of By Versus RF Power.

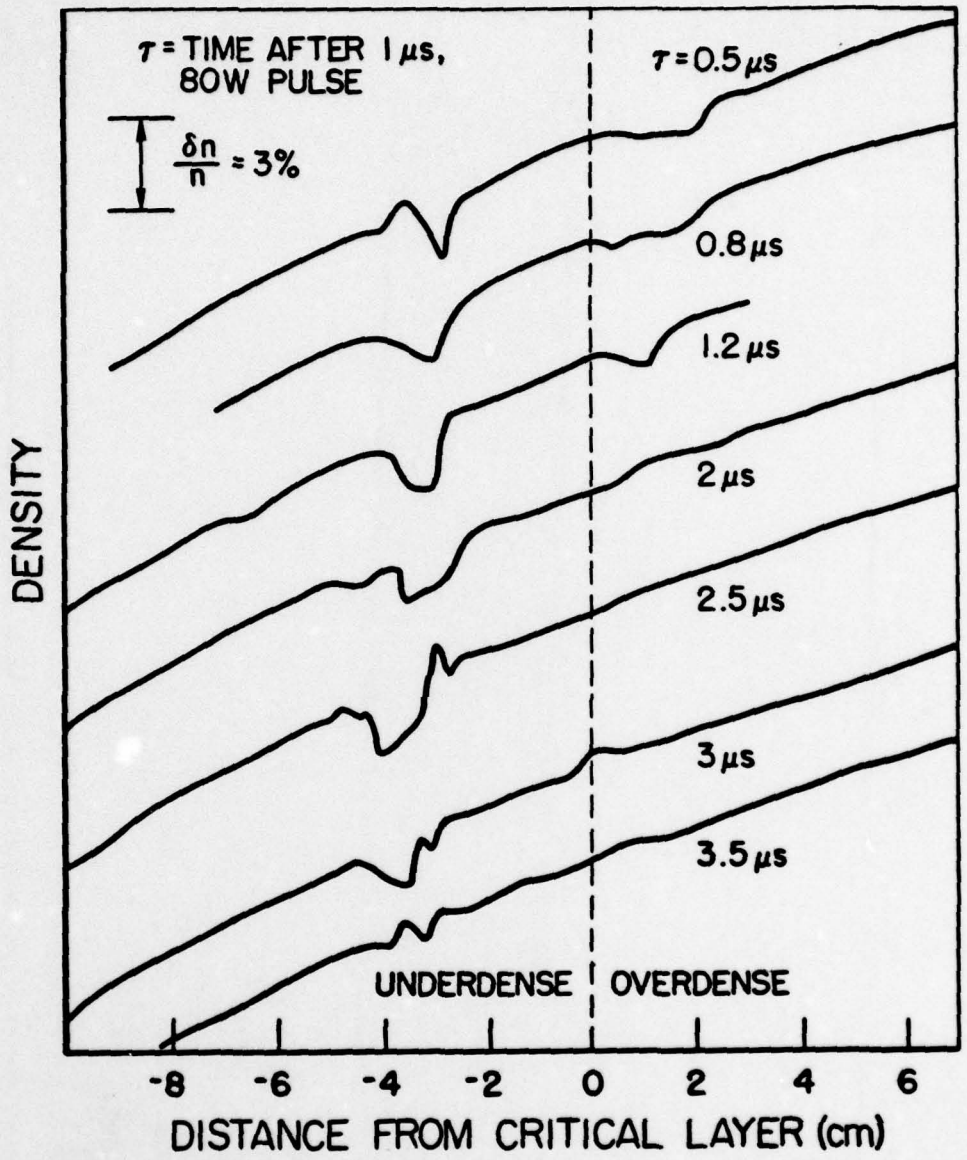

Fig. 8. Perturbed Density Profile.

density change. It should be noted that the actual width and depth of the density cavity are probably significantly different from the measured values due to the probe perturbation of the resonance region. However, the formation of a density cavity suitable for plasma wave trapping is clearly seen. Future plans include the use of electron beam probing to measure the actual width of the cavity.

Measurements were made of the high frequency rf electric fields using both monopole and dipole probes. Time resolved measurements of the rf electric field in the vicinity of the resonance layer reveal that both the rf electric field and quasi-static magnetic field saturation times are coincident (see Fig. 9). The peak of the electric field near the resonance layer was found to be located in the center of the aforementioned stationary density cavity. By employing input rf pulses with sharp leading and trailing edges ($\tau < 10$ nsec) we were able to observe a difference in the field growth and decay characteristics in the neighborhood of the cut-off and resonance layers, respectively. Specifically, we find that the pulse shape in the vicinity of the cut-off layer exactly follows the input rf pulse to within the limits of resolution of our system ($\simeq$ 25 nsec). However, the temporal behavior is quite different in the neighborhood of the critical layer. We find that the field rises much more slowly than the incident rf pulse and that it decays more slowly than the incident rf pulse which is suggestive of wave trapping in

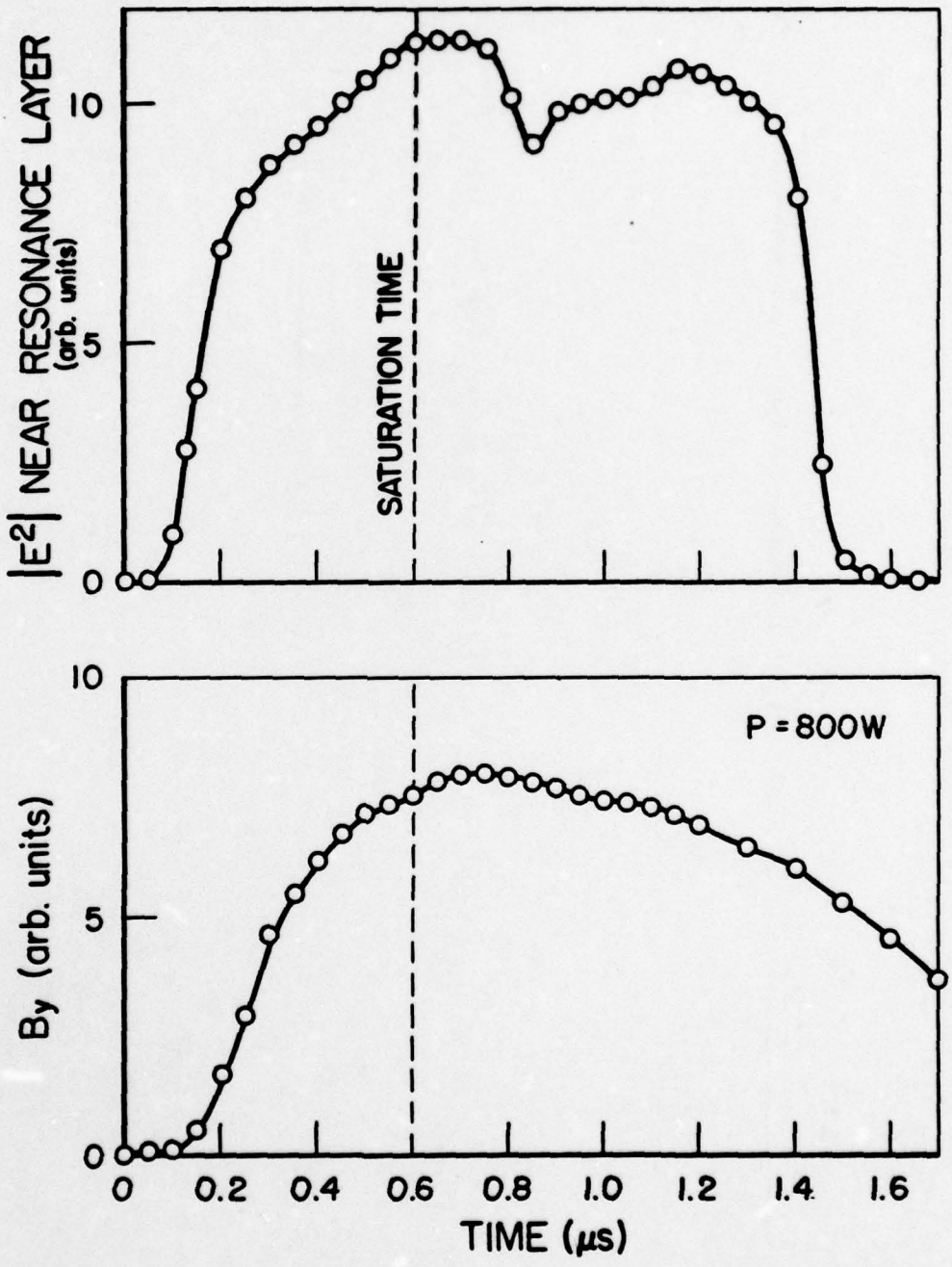

Fig. 9. Coincidence of Saturation Times for Electric and Magnetic Fields.

the previously described density cavity. It should be again stressed that the presence of the probe strongly perturbs the resonance layer and can serve as a loss mechanism for electron plasma waves. Therefore, the observed trapping time of 75 nsec (for $|E^2|$) at 50 W is probably much smaller than the actual value. Again, it appears that electron beam probing will be required to remove the discrepancy.

The scaling of the saturated value of the electric field in the vicinity of the critical layer was also measured. Here the probe was typically located at resonance. The saturated electric field exhibits a sharp break in scaling at a power level of $\simeq$ 40 W identical to that exhibited by the magnetic field. However, we note that where B_{sat} changes from a p^1 to p^2 dependence, E_{sat} changes from a $p^{2.2}$ to a $p^{0.4}$ dependence. Additional work must be done until these latter dependences are understood.

As discussed above, the measured saturation level and saturation time for the quasi-static magnetic field are approximately 100 and 10 times, respectively, the predictions of Speziale and Catto[7]. Furthermore, the measured spatial variation of the magnetic field is much more gentle then the predicted variations. We have numerically plotted the magnetic field using the expression of Ref. 7 evaluated at τ = 700 nsec and find that the field is primarily restricted to a narrow region near the critical layer. To better understand the disparity between experiment and theory we first carefully examined the

assumptions of their model. We then proceeded to derive our own theoretical expressions for the magnitude and spatial dependence of the saturated magnetic field.

Speziale and Catto[7] obtain the magnetic field by integrating the beat current $-e\langle nu\rangle$ from ∞ to x (axial position along the density gradient) under the assumption that β vanishes at $x = \infty$. They obtain the high frequency field via Laplace transformation (initial valve problem) with a solution restricted to the region $(\omega_p - \omega_o)/\omega_o \ll 1$ (i.e. near the critical layer). As mentioned above, the spatial distribution of the magnetic field predicted by this model is much more narrow than the measured field variation.

To resolve this disagreement we have investigated the saturated magnetic field in the low power linear regime where analytic solutions may easily be obtained. Since our measured angle of incidence is rather small ($\theta \simeq 14^o$) the large angle expressions for the high frequency fields given by Ginzburg are not applicable. We therefore obtained an exact series solution similar to that of Förster ling by assuming $E \propto f(x)\ e^{i\omega_o t - ik_y y}$ and Fourier transforming the coupled fluid-Maxwell equations. The high frequency longitudinal electric field in the underdense region then has the form

$$E_x = C_1 \sum_{n=o}^{\infty} a_n \delta^{n+1} + C_2 \left[\frac{q^2}{2} (\ln\delta) \sum_{n=o}^{\infty} a_n \delta^{n+1} + \sum_{n=o}^{\infty} b_n \delta^{n-1} \right] \quad \text{where } q^2 = k_o^2 \sin^2\theta,$$

$\delta = \varepsilon L$, L is the density gradient scale length and ε is the plasma dielectric constant. In the overdense region (near the critical layer) we have $E_x = C_3 \delta^{-1}$. To obtain the coefficients we employ the following boundary conditions:

(1) At the horn $E_x = E_o \sin\theta$

(2) At the critical layer, both electric field and its derivative must be continuous. The perpendicular electric field was obtained utilizing

$$E_y = (1/ik_o \sin\theta)\ (E_x + E_x \frac{\varepsilon^1(x)}{\varepsilon(x)} \qquad \text{where}$$

the prime denotes differentiation with respect to x. Maxwell's equations yield

$$\frac{dB}{dx} = \frac{4\pi e}{c} \quad \langle nu_y \rangle \qquad \text{with}$$

$$- 4\pi en = \frac{dE_x}{dx} - iky\ E_y$$

We note that Speziale and Catto[7] ignored the $ik_y E_y$ term in their derivation. We find that the model described above well describes our experimental measurements. First, the predicted longitudinal electric field is in good agreement with out low power ($\eta_{vac} \leq 1.4 \times 10^{-4}$) experimental results. In addition, the theory predicts a large current sheet perpendicular to the density gradient located at the resonance layer. This current sheet is the main contribution to the d.c. magnetic field generation. The magnetic field will therefore change sign near the critical layer, slowly vary spatially and

attain its largest value near the critical layer, all in agreement with experiment. Figs. 10 and 11 display the spatial variation of $|E|^2$ and the current sheet for an incident angle $\theta = 10^o$. The magnitude of the magnetic field is easily obtained by integration of the current sheet. The predicted value is approximately an order of magnitude larger than the measured value. The various field saturation terms are presently being examined to see if this discrepancy can be resolved.

3. Soliton Flash

The absorption mechanism for electromagnetic waves near the critical layer becomes more complicated at powers in excess of those utilized for the measurements described in the preceeding subsection.

Elsasser and Schamel[8] have proposed that strong ion heating can occur due to the strong fields associated with a transient solitary wave structure which they call the "soliton flash." We have observed such behavior in our plasma. The field maximum typically occurs at $\omega_{pi}\,\tau \simeq 20$ after the turn-on of the rf as compared to $\omega_{pi}\,\tau \simeq 10$ as predicted by Elasser and Schamel. Figure 12 shows that the flash time scales as ω_{pi}^{-1} as predicted. A comparison of our electric field time evolution with their numerical predictions is shown in Figure 13. We also note that as shown in Figure 14 the quasi-static magnetic field exhibits a growth whose maximum is correlated with the "soliton flash." A similar correlation in the hot electron production is observed as indicated in Fig. 15. A preliminary description

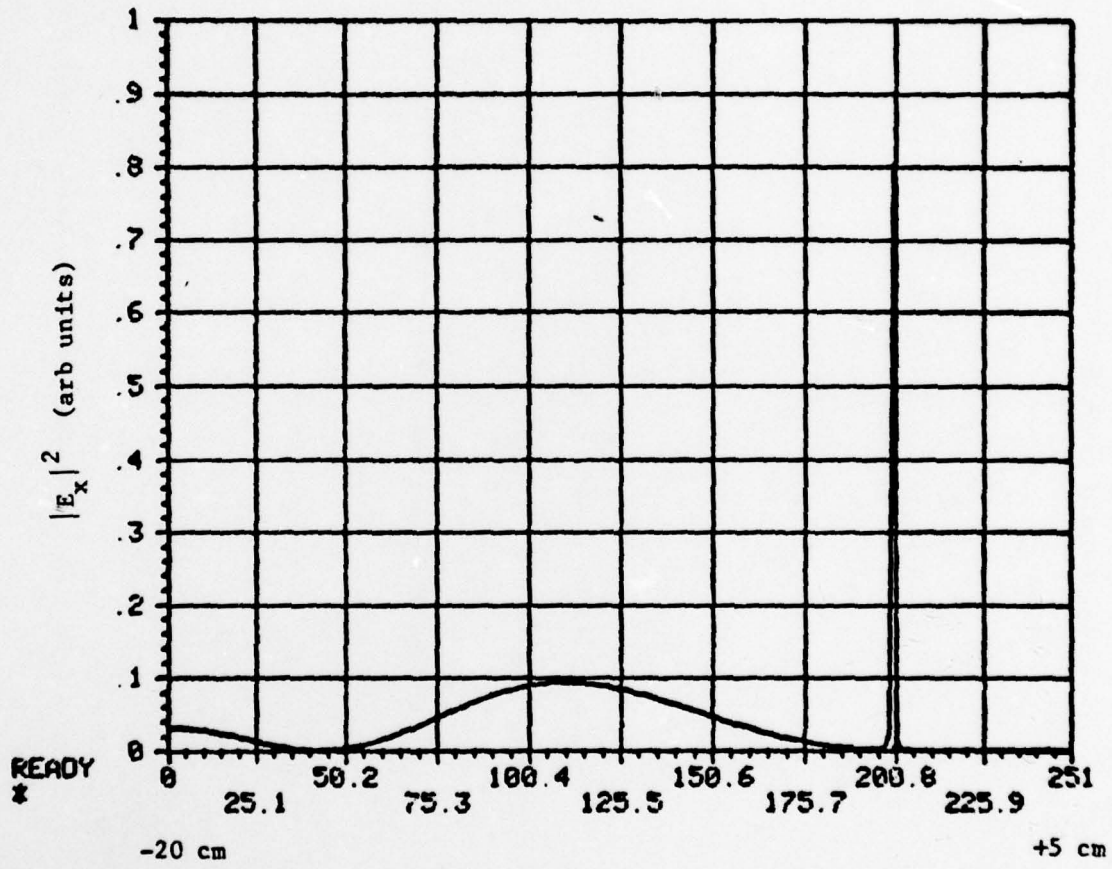

Fig. 10. Spatial Variation of $|E_x|^2$

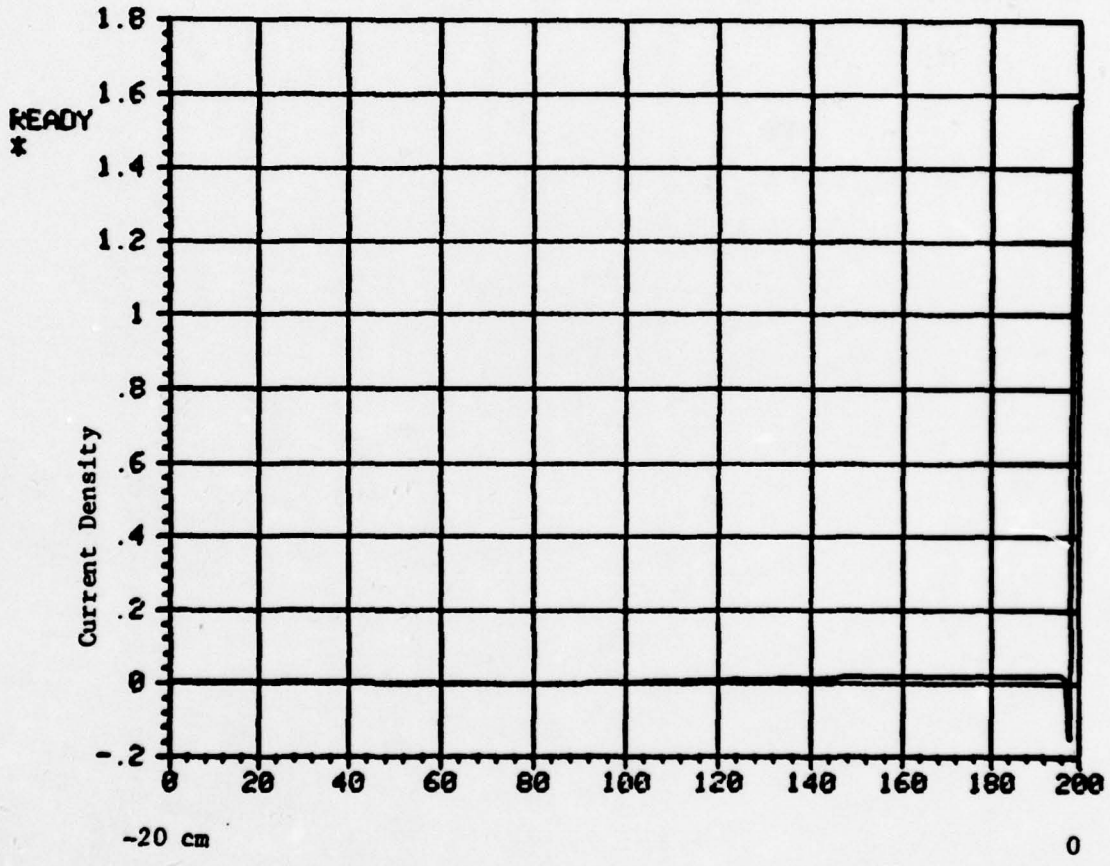

Fig. 11. Spatial Variation of Current Density

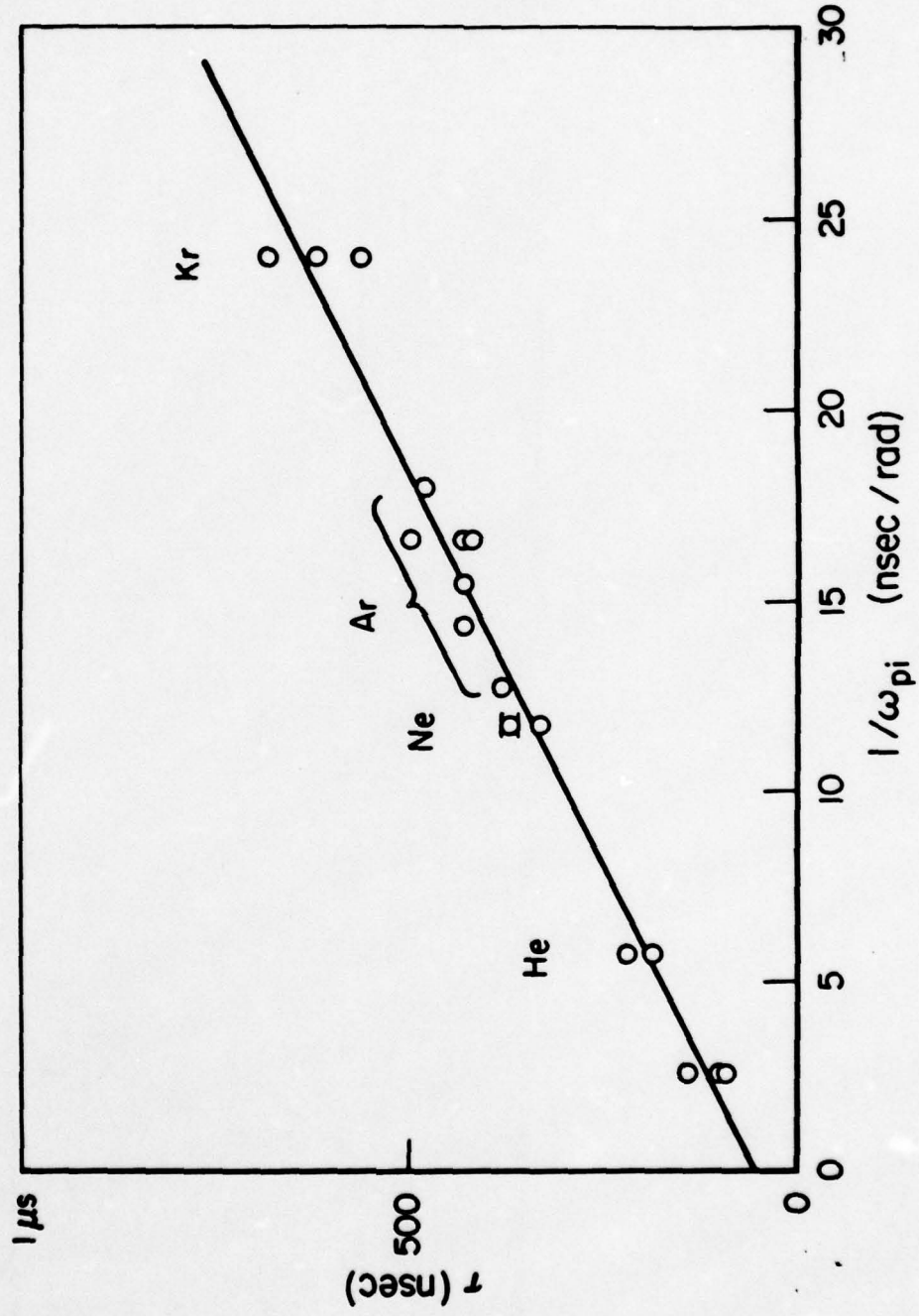

Fig. 12. Ion Mass Dependence of Flash Time

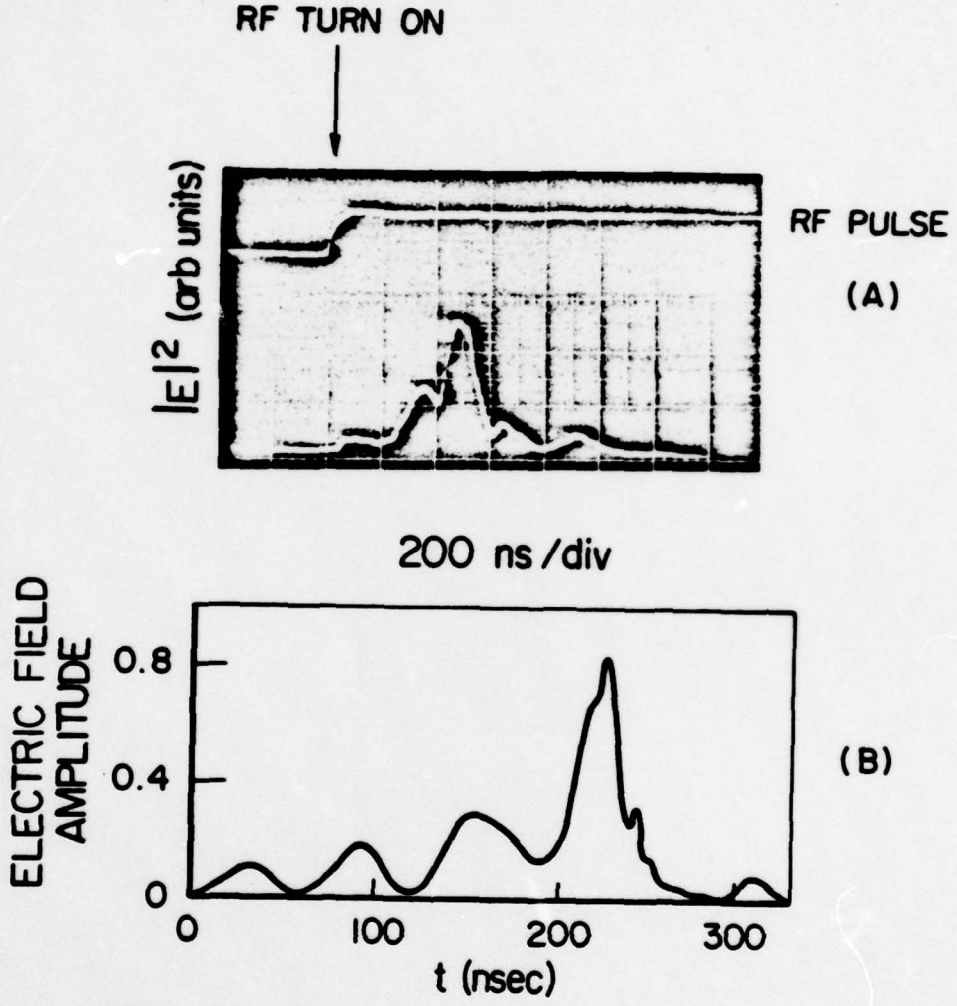

Fig. 13. Comparison of Experimentally Measured Electric Field Intensity Near Critical Layer with Predictions of Elsasser and Schamel.

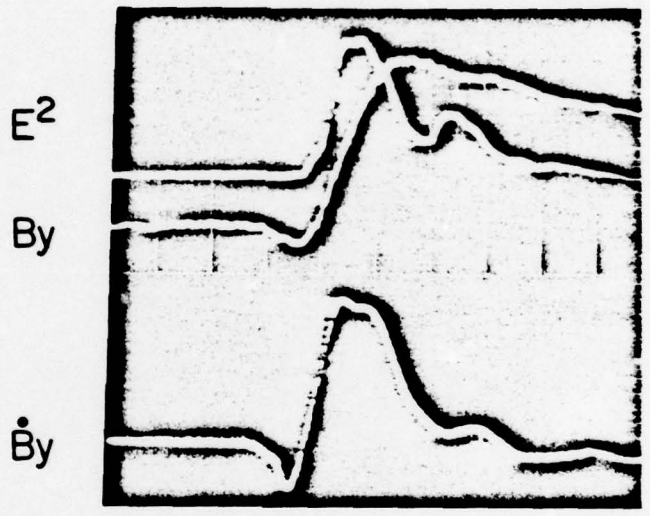

Fig. 14. Correlation of Magnetic Field Behavior with "Soliton-Flash."

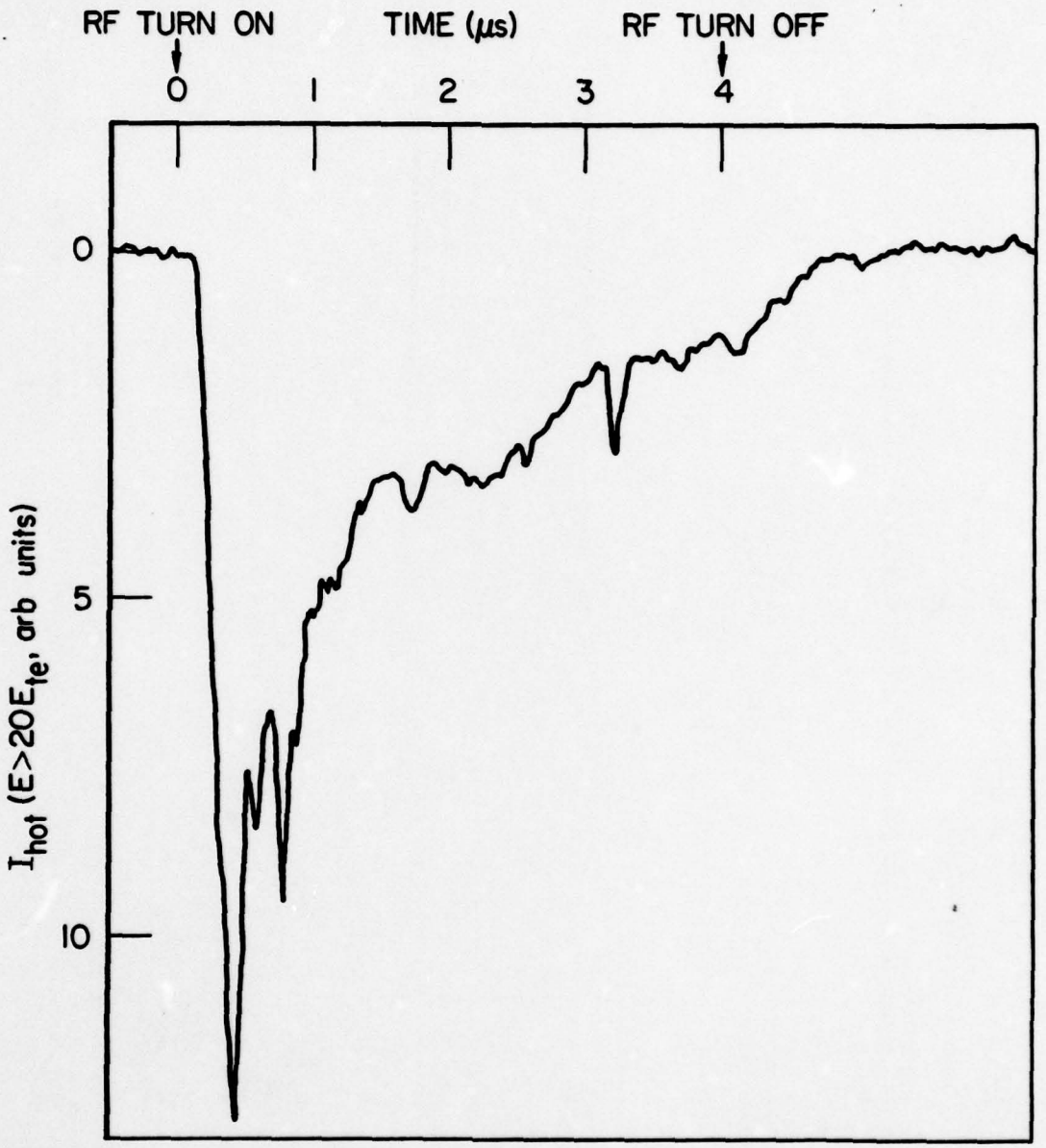

Fig. 15. Correlation of Hot Electron Production with "Soliton Flash"

of these observations has been prepared for submission to Physical Review Letters and is included as Appendix II. We hope to refine these measurements during the coming year. We note that, although these transient phenomena may not necessarily be as important as say SBS studies to laser fusion, they shed additional light on the complicated processes associated with energy absorption at the critical layer.

B. Acquisition and Testing of MORT and AWACS S-band Radar Systems For Microwave Simulations of Laser Plasma Interactions

In order to increase the field intensities for our microwave investigations of laser-plasma interactions, we located two S-band radar transmitters which were transferred to our contract. The lower power ($P \simeq 160$ kW) MORT radar is primarily being used in our critical density plasma. The higher power AWACS system ($P \simeq 1.5$ MW) will be used in finite bandwidth studies of backscattering instabilities.

The MORT radar system was delivered to us inside a 40-foot long trailer. The documentation was also inside the trailer and was found to be complete including test procedures for most components. The transmitter group was removed from the trailer and reassembled in our laboratory. Power was supplied by existing 400 Hz motor generators. The system was found to be in working order for the most part, and was brought online in December 1978. The transmitter was found to produce a 10 μsec RF pulse at a peak power of 160 kW as specified in the documentation. The output was routed via a switchable waveguide transmission line to two of our plasma chambers.

The AWACS Radar was delivered to us as a completely disassembled system without any documentation. We requested (from Hughes) documentation and subsequently received an incomplete set of prints. After finding these prints inadequate to assemble the transmitter, we issued a second request for documentation. The new set of prints arrived in March 1979.

The second set of prints were complete enough to allow us to assemble the transmitter portion of the AWACS. Assembly was begun in June 1979. The AWACS required an increase in our 400 Hz power capability. This was accomplished by replacing our motor generator sets with more powerful models.

The water cooling system was not supplied to us so we constructed our own. The tank containing the high voltage regulator was delivered to us unpressurized so we pumped it out, purged it, and backfilled it with dielectric freon. All the required interlocks were satisfied and switches were added to control functions previously controlled from the ECCM panel.

Various problems were encountered in trying to bring the AWACS into operation including coolant leaks and defects in the inverter trigger circuitry.

A timing circuit was constructed to generate the transmitter on and off signals. This circuit included a 10 Hz internal clock rate and an external triggering capability to facilitate synchronization with our pulsed plasma discharge.

The RF output was connected to our plasma chamber via a waveguide system. This included the AWACS duplexer to protect the third RFA from reflected power, a harmonic rejection filter, two directional couplers to measure forward and reverse power, a ceramic window, and various bends. We found it was necessary to pressurize the waveguide with SF_6 because of arcing inside the harmonic rejection filter. Since our pulse shape requirements were different from the original AWACS design, the pulse shape and phase control portions of the first RFA were bypassed. In addition, we found that output stability was enhanced by adding an RF isolator between the second and third RFA's.

The system has been tested and delivers 1MW of RF power to our chamber between 3.25 and 3.35 GHz. Experiments are now in progress.

C. Finite-Beta Waves and Instabilities

Basic plasma physics experiments with applications toward magnetospheric physics require controlled laboratory plasmas with known parameters. For experiments dealing with long wavelength instabilities, rf absorption and heating, current driven instabilities and laser microwave diagnostics, considerable effort has been spent in generating a 3-meter long, 5 cm diameter magnetized plasma. Requirements of this system include a density greater than 10^{13} cm^{-3}, plasma production independent of any axial currents, and steady state operation in the 2 kG axial magnetic field.

The primary problem in the construction of such a device is the plasma generation system. The Lanthanum Hexaboride hollow cathode developed at UCLA provided a good starting point due to its high ionization capabilities and steady-state operation at large currents. This cathode was placed 20 - 40 cm from a cylindrical anode at one end of the vacuum system and a discharge up to 350 A between the two produced the required plasma in A, He & H. This plasma drifted along the axial magnetic field and was collected on a water cooled electrode (at the far end) which could be individually biased to collect any current desired.

Several variations of this basic design have been tried in the continuing effort to expand the plasma diameter without sacrificing the density or component lifetimes. These configurations will be discussed along with the studies of the plasma discharge and some preliminary observation of the plasma instabilities.

1. Cathode-Anode Assembly

The cathode for this device is a hollow tungsten tube with an indirectly heated solid lanthanum hexaboride element inside as the active electron emitter. Neutral gas is fed into this tube and exits from a small aperture at the front. The neutral gas pressure inside the tube, and therefore the plasma density and collisionality, is controlled by the gas flow and the aperture diameter. The cathode was operated directly in the 2 kG axial magnetic field and in a field free magnetic cusp generated by current reversal in the last field coil.

Operation in the field free (or low field) region produced a discharge of 50 - 350 A at 40 - 90 V in A and 60 - 110 V in H:He. The cathode aperture diameter was varied between 0.5 cm - 1.25 cm, with the most efficient, low noise operation obtained at a diameter of about 0.65 cm. In the magnetic field, the aperture diameter had to be .5 - .65 cm in order to draw more than 100 A from the cathode. This is attributed to the increased collisionality of the cathode plasma required for proper operation. However, bombardment of the tungsten shell by the dense, axially confined plasma (flux) caused serious overheating and evaporation of the cathode components and limited the system lifetime to about 25 hours.

Three anode assemblies were tested in the attempt to generate a high density, 5 cm diameter plasma column. The first was simply a cooled surface at the point where the cusp magnetic field strikes the chamber wall. The plasma generated in this configuration had the required density, but was less than 1 cm in diameter. Expansion of the plasma diameter was accomplished by moving the anode and cathode into the high magnetic field region. The anode had a diameter of 1.25 cm and fully enclosed the cathode so that the gas flowed through both cathode and anode orifices.

The anode was placed so that the maximum magnetic flux passed through the aperture, and the generated plasma expanded to about 3 cm in diameter in the slightly lower field of the 3-meter vacuum system.

The system parameters for this configuration are:

Magnetic field on system axis	2 kG
Gas	Argon
Background chamber pressure (measured	$2\text{-}3 \times 10^{-4}$ Torr
Anode interior pressure (calc)	2×10^{-3} Torr
Cathode interior pressure (calc)	1×10^{-2} Torr
Discharge current	50 - 300 A
Density	$> 10^{13}$ cm^{-3}
Electron Temp.	between 2-5 eV

Operation in helium and hydrogen was very similar but required about twice the gas pressure and 10 volts higher discharge voltage.

The plasma was further expanded in diameter by the construction of a wheel shaped anode with a 3 cm in diameter orifice. This anode consisted of six copper water lines bent and soldered from a cooled orifice.

The larger anode expanded the plasma diameter in Ar to about 4.5-5 cm at a density of 1.5×10^{13} and a discharge current of 250A.

In the attempt to generate the high density, large diameter plasma using the LaB_6 hollow cathode in this configuration, several scaling rules became apparent. The anode should be in the highest magnetic field region as this will determine the plasma diameter. In the cathode in the magnetic field, the largest aperture gives the largest plasma. However, if the aperture becomes too large (> 7 cm), the

collisionality of the cathode plasma decreases and the cathode ceases to operate at high current. For the cathode in the field-free cusp, the aperture can be opened until the cathode plasma density decreases enough to limit the extracted electron current. Since the cathode is in a low magnetic flux region, electrons must diffuse across the field lines to strike the anode and generate the large diameter plasma. This can be accomplished by aperture limiting at the anode to increase the neutral gas density in the discharge region and collisionally diffusing the plasma to the anode ring. The discharge voltage also rises in this case since the perpendicular diffusion is also aided by high energy electrons. ($D \propto KT$ for electron-neutral collisions). The best configuration is a cooled anode in the maximum magnetic field in which all the gas passes through the aperture, and the cathode in the decreasing field of the cusp field so that the plasma flux decreases enough to allow reasonable component lifetimes.

2. Plasma Column Modifications

In the original construction of the long plasma column vacuum system, a 7.5 cm diameter constriction was placed in the machine center to accommodate the magnetic field coil system. As the plasma diameter increased, this constriction overheated and limited the running time to about 5 minutes. Current work is involved in the removal of the constriction and modification of this section of the chamber to a minimum 15 cm diameter. At the same time, the advantageous discharge configur-

ations mentioned in the last section is being re-constructed with proper cooling for higher current operation (500 A). It is anticipated that these modifications will produce a > 5 cm diameter, 10^{13} cm^{-3} plasma in helium capable of steady state operation.

3. Plasma Oscillations

Preliminary investigation of the oscillations present in this plasma column under certain discharge conditions revealed at least two different instabilities and suggested that more were present. Diagnostics were performed using Langmuir probes placed just outside the main plasma column. A large amplitude, low frequency wave was present at just about all discharge currents and for chamber pressures below 5×10^{-4} Torr. Biasing the probes to collect ion saturation current indicated that this rotating wave (azimuthal, m = 1) had a density about equal to that of the main plasma column. The instability had a frequency of 9.2 kHz, a wavelength of 1 meter, and rotated with an azimuthal phase velocity of 1.8×10^{5} cm/sec. A calculation of the electron diamagnetic drift velocity coincided with this value assuming a 5 eV electron temperature, suggesting that this is a drift wave. At discharge currents above 300 A corresponding to densities well over 10^{13} cm^{-3}, this instability decreased in magnitude and the plasma became much quieter. Decreasing the gas pressure below 2×10^{-4} Torr at this current restores the instability.

A second instability was detected at 600 kHz but was not investigated in detail. During all of these tests, the cooled electrode at

the end of the system was allowed to float. Future experiments will involve investigation of other instabilities already present and current driven instabilities produced by biasing the end electrode. More sophisticated diagnostics such as FIR laser scattering and spectroscopy are being moved into position for use on this machine at this time.

D. Plasma Diagnostic Development

The strength of our program continues to be due to our strong emphasis on diagnostics development. Particular attention has been paid to measurements associated with microwave simulations of laser-plasma interactions.

1. RF Synchronized Plasma Pulser

A master timing circuit has been designed and constructed that enables us to launch coherent 3 GHz wave packets into a plasma. The wave packets are viewed directly using a sampling oscilloscope. The sampling time base produces a 28 KHz square wave that is used to synchronize the entire system. The 28 KHz signal is divided down to 10 Hz and a series of delay channels trigger the plasma, the RF modulator, the RF signal source, and other oscilloscopes. All of these events are synchronized to the sampling unit. In another mode of operation the timer is internally clocked with a variable repetition rate of 5 to 20 Hz. This mode is used for experiments that do not require the sampling unit.

2. Boxcar Data Acquisition System

We have completed construction and testing of the Boxcar Data Processor (BDP). This device digitizes the analog output of our boxcar integrator and inputs the data to our H.P. 9825A programable calculator for analysis and storage. The following is a general description of the BDP design followed by a detailed explanation of the circuit functions, timing, and logic.

Figure 16 is a block diagram of the Boxcar Data Processor (BDP). Two inputs are required from the boxcar. The analog output is connected to the analog to digital converter (A/D), and the scan output is connected to the comparator as shown in Fig. 16. The boxcar scan output produces a signal that increases from 0 to 10 volts as the boxcar sampling gate scans across the time base. The staircase generator is comprised of an 8 bit counter driving a digital to analog converter (D/A). This voltage is compared to the scan ramp in the comparator. The comparator output triggers the sampling sequence of the A/D and subsequent transfer of data to the calculator. Since the staircase has 256 steps, a full scan yields 256 data samples. The A/D produces a 10 bit word. The coding is such that all zeroes corresponds to -5 volts and all ones corresponds to +5 volts. With the boxcar on its most sensitive scale a resolution of .05 mV is obtained.

The details of the circuit logic are now described. The schematic diagram is shown in Fig. 17. With the boxcar ready for a scan,

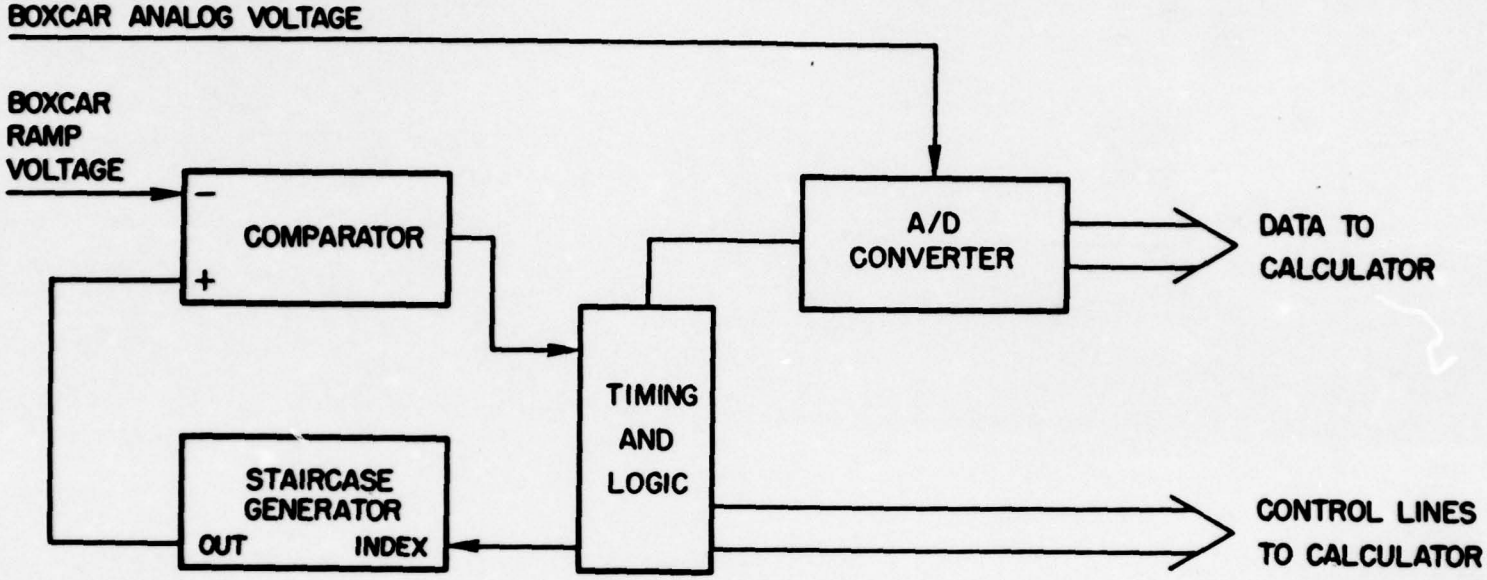

Fig. 16. Boxcar Data Processor.

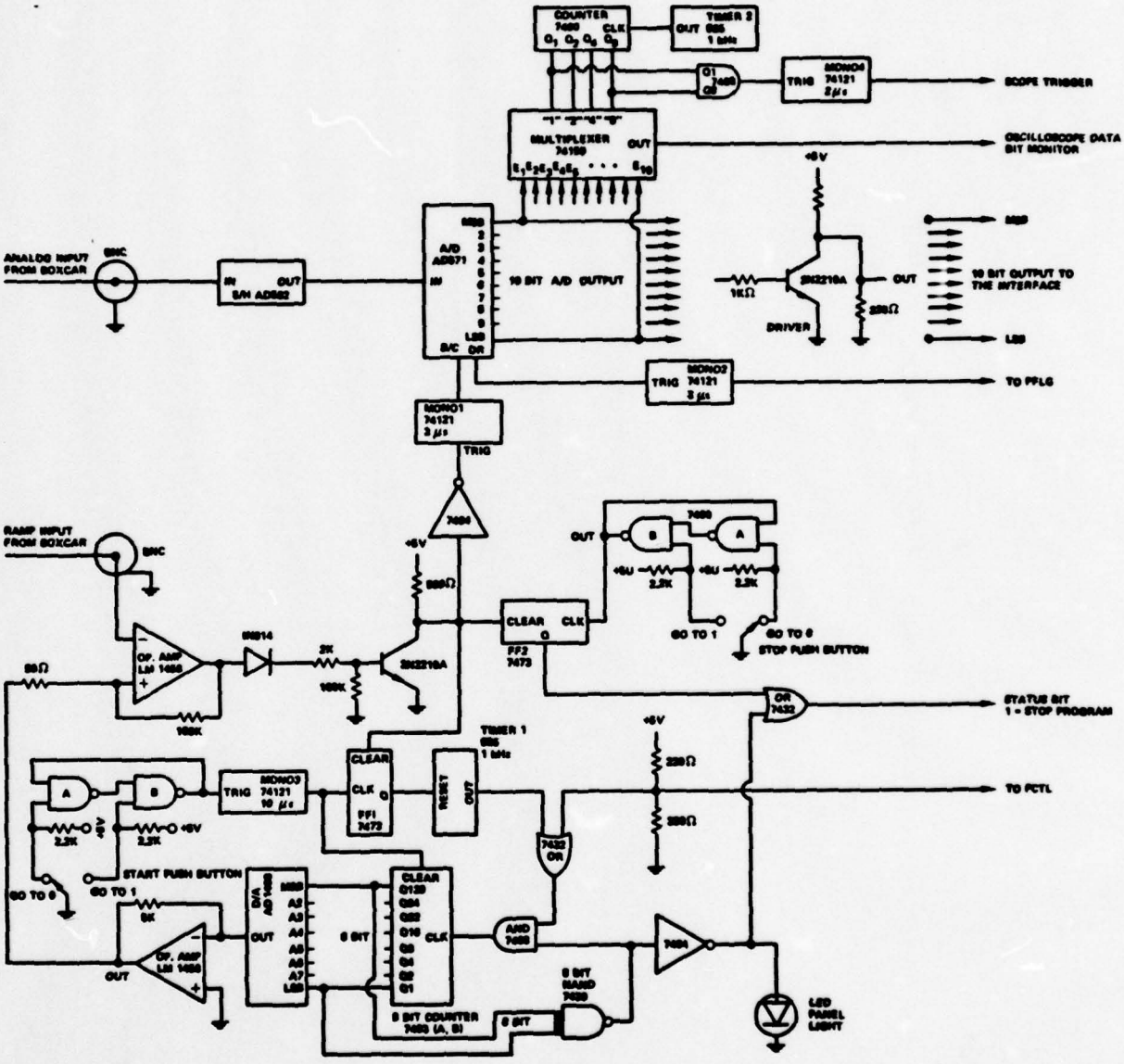

Fig. 17. Detailed Schematic Diagram of Boxcar Data Processor.

the reset button is pushed. The switch drives a contact debouncer and goes from high to low. This triggers monostable 3 which generates a positive pulse. The leading edge of this pulse resets the staircase generator to zero volts. The trailing edge boggles flipflop 1 which enables clock 1. Clock 1 generates a 1 KHz pulse train. The trailing edge of these pulses indexes the staircase until the staircase voltage is higher than the boxcar ramp. At this point the comparator goes from high to low, clearing FF1 which stops the pulses from clock 1. The comparator is comprised of an op amp using regenerative feedback to give a Schmidt trigger action with a small amount of hysterisis for noise immunity. The tranistor is a level converter to bring the op amp output down to TTL level.

The system is now ready to accept data. The scan is started and when the ramp increases by 40 mV the comparator goes from high to low. This triggers mono 1 which generates a 3 μs pulse. The leading edge blanks the A/D output and the trailing edge starts a new conversion. After about 25 μs the data ready line goes from high to low. This triggers mono 2 which drives the PFLG line to the calculator. This tells the calculator that data is ready to be read from the converter. The data lines to the calculator are buffered with transitor line drivers. When the calculator has accepted the data it drives the PCTL line from high to low indexing the staircase. The comparator goes low and the circuit waits for the boxcar ramp to increase another 40 mV.

When the staircase reaches its highest step, the eight input NAND gate goes low which inhibits additional indexing commands from PCTL. The stop button can be used to set a status bit which is monitored by the program running in the calculator and interpreted to mean: stop the program. The scope display circuit is comprised of a 10 line to 1 line multiplexer which is clocked every millisecond. The AND gate together with mono 4 generate synchronizing trigger pulses for the oscilloscope. This gives a clear display of the binary word on the A/D output lines.

The circuit was built on a 9" x 6" integrated circuit breadboard using wire wrapping for interconnection.

The BDP is currently being used in our study of critical layer phenomena and an article concerning the design will be submitted to the Review of Scientific Instruments for publication.

3. Electric Dipole Probe

We have constructed a directional electric dipole probe with a high-input impedance to measure the electric field enhancement in the neighborhood of the cut-off and critical layers. It is hoped that its small size ($\simeq$ 1 cm diam.) combined with high input impedance will minimize the perturbation of the plasma, particularly in the neighborhood of the resonance layer. The two dipole legs feed a shielded, balanced transmission line with a characteristic impedance of 100 Ω. At the desired frequency f_o this line is $\lambda/4$ long and is terminated by a 4Ω

high frequency (low inductance) resistor. Thus the input impedance is 2500Ω. The following section of transmission line is simply an impedance transformer to match the 4Ω resistor to a standard 50 transmission line.

4. Retarding Grid Energy Analyzer

Suprathermal electrons and ions generated in our microwave simulation experiments are detected using an electrostatic multigrid retarding energy analyzer. The energy analyzer (.76 cm long, 1.5 cm diam.) body is machined from solid copper to reduce the possibility of spurious signals due to the presence of the strong microwave fields. The first grid (98 lines/mm) which is held at the body potential, provides an additional rf attenuation. This shielding is so successful that the analyzer can actually be inserted into the underdense plasma region inside the horn without encountering spurious pickup.

III. PUBLICATIONS, REPORTS AND PRESENTATIONS (October 1, 1978 - September 30, 1979)

1. "Self-Magnetic Field Generation in a Plasma," S. P. Obenschain and N. C. Luhmann, Jr., Phys. Rev. Lett. 42, 311 (1979).
2. "Instrumentation and Techniques for Plasma Diagnostics: An Overview," a chapter to appear in Vol. II of Infrared and Submillimeter Waves (Academic Press) edited by K. J. Button, 1979. Also UCLA PPG-381.
3. "The Development of a High Frequency Correlator for the Study of Plasma Turbulence," C. K. Chan, UCLA-ENG-7868, October 1978.
4. "Annual Scientific Report," UCLA-ENG-7891, November 1978.
5. "Annual Scientific Report," UCLA-ENG-7908.
6. "Profile Modifications and Magnetic Field Generation Due to Intense Microwave Plasma Interaction," Y. Nishida, S. P. Obenschain and N. C. Luhmann, Jr., Bull. Am. Phys. Soc. 23, 886 (1978).
7. "Observation of Stimulated Brillouin Scattering in Microwave Plasma Interactions," H. E. Huey, A. Mase, N. C. Luhmann, Jr., and C. Pauley, presented at 1979 IEEE International Conference on Plasma Science, Montreal, Canada, June 1979.
8. "Generation of Magnetic Fields in Microwave Experimental Simulation of Laser Fusion Interactions," M. Rhodes, Ann Y. Lee, N. C. Luhmann, Jr., S. P. Obenschain and Y. Nishida, presented at 1979 IEEE International Conference on Plasma Science, Montreal, Canada, June 1979.

9. "Resonance Absorption Produced Quasi-Static Magnetic Fields," M. Rhodes, Ann Y. Lee, N. C. Luhmann, Jr., Y. Nishida, and S. P. Obenschain, presented at the 9th Annual Conference on Anomalous Absorption of Electromagnetic Waves, Rochester, New York, May 16-18, 1979.

10. "Microwave Experimental Studies of Stimulated Brillouin Scattering," H. E. Huey, A. Mase and N. C. Luhmann, Jr., presented at 9th Annual Conference on Anomalous Absorption of Electromagnetic Waves," Rochester, New York, May 16-18, 1979.

11. "Observation of Stimulated Brillouin Scattering in a Microwave Plasma Interaction Experiment," H. E. Huey, A. Mase and N. C. Luhmann, Jr., submitted to Phys. Rev. Letters, also UCLA Report PPG-422.

12. "UCLA Microwave Simulation Program," Invited Talk presented at Conference on Microwave Modeling of Laser Plasma Interactions, TRW, June (1979).

13. "Observation of the Soliton Flash," M. Rhodes, Ann Y. Lee, Y. Nishida, N. C. Luhmann, Jr. and S. P. Obenschain, submitted to Phys. Rev. Letters, also UCLA Report PPG-428.

14. "Effects of Finite-Bandwidth Pump on Stimulated Brillouin Scattering," A. Mase, H. Huey, M. Rhodes, N. C. Luhmann, Jr., to be presented at the 1979 APS Plasma Divisional Meeting, to be held in Boston, Mass., November 1979.

15. "Observation of Soliton Flash," M. Rhodes, Ann Y. Lee, Y. Nishida, and N. C. Luhmann, Jr., to be presented at the 1979 APS Plasma Divisional Meeting, Boston, Mass., November 1979.

16. "Magnetic Field Generation in a Microwave-Plasma Interaction Experiment," Ann Y. Lee, M. Rhodes, Y. Nishida, N. C. Luhmann, Jr., and S. P. Obenschain, to be presented at the 1979 APS Plasma Divisional Meeting, to be held in Boston, Mass., November 1979

17. "Observation of Stimulated Brillouin Scattering in a Microwave Plasma Experiment," H. Huey, A. Mase, C. Pauley, and N. C. Luhmann, Jr., to be presented at the 1979 APS Plasma Divisional Meeting, to be held in Boston, Mass., November 1979.

IV. RESEARCH PERSONNEL

1. N. C. Luhmann, Jr.
2. F. F. Chen
3. Professor Kawaguchi (Visitor, Mie University, Japan).
4. Professor Nishida (Visitor, Utsunomiya University, Japan).
5. Professor Ohnuma (Visitor, Tohoku University, Japan).
6. A. Lee (Graduate Student).
7. H. Huey (Graduate Student).
8. D. Goebel (Graduate Student).
9. M. Rhodes (Graduate Student).

V. REFERENCES

1. D. Pesme, G. Laval, and R. Pellat, Phys. Rev. Lett. 31, 203 (1973).
2. C. S. Liu, M. N. Rosenbluth, and R. B. White, Phys. Fluids 17, 1211 (1974).
3. D. W. Forslund, J. M. Kindel, and E. L. Lindmen, Phys. Fluids 18, 1017 (1975) and many references to early work.
4. A. A. Offenberger, M. R. Cevenan, A. M. Yam, and A. W. Pasternak, J. Appl. Phys. 47, 1451 (1976).
5. B. H. Ripin, F. C. Young, J. A. Stamper, C. M. Armstrong, R. Decoste, E. A. McLean, and S. E. Bodner, Phys. Rev. Lett. 39, 611 (1977).
6. D. W. Phillion, W. L. Kruer, and V. C. Rupert, Phys. Rev. Lett. 39, 1529 (1977).
7. T. Speziale and P. I. Catto, Physics of Fluids, 21, 2063 (1978).
8. K. Elsässer and H. Schamel, Plasma Physics 19, 1055 (1977).

OBSERVATION OF STIMULATED BRILLOUIN SCATTERING IN A MICROWAVE PLASMA INTERACTION EXPERIMENT

H. E. Huey, A. Mase* and N. C. Luhmann, Jr.

University of California, Los Angeles, CA 90024

Stimulated Brillouin scattering of microwave radiation is investigated in an underdense laboratory plasma. The energy and momentum selection rules are seen to be satisfied for a variety of incident wavelengths (λ_o = 3 ~ 10 cm) and ion species (He, Ne, Ar and Kr). The threshold power, growth rate and scattered power appear to be consistent with the finite interaction length theory. Saturation of the backscatter is observed and compared with existing theories.

---

*Permanent Address: Faculty of Engineering, Nagoya University, Nagoya, 464, Japan

Stimulated Brillouin scattering (SBS) is a serious obstacle preventing the efficient absorption of the incident laser light in laser pellet interaction experiments[1-5]. We report here the first observation of SBS in a microwave-plasma interaction which may help to elucidate some of the physics relevant to the laser-plasma case. Specifically, the threshold power, growth rate, and saturation level have been determined for SBS in a 0.1 n_{cr} plasma.

The experiments were performed in an unmagnetized plasma of 75 cm diameter and 2 m length produced by a multi-filament discharge with surface multipole magnetic confinement. Typical operating parameters are gas filling pressure $1 - 3 \times 10^{-4}$ Torr, electron density $n_o = 10^{10} \sim 10^{11}$ cm^{-3}, density gradient scalelengths $L/\lambda_o \simeq 20 - 70$, temperature $T_e \simeq 2$ eV, and electron-ion temperature ratio $T_e/T_i \simeq 10 \sim 12$. The microwave pump of frequency $\omega_o/2\pi = 3.4 \sim 16$ GHz, power $P \lesssim 1$ MW and pulse width $\tau_p = 0.1 \sim 10$ μsec is introduced along the chamber axis by means of a high gain ($\simeq 20$ dB) gridded horn. For the experiments described herein, n_o was maintained at 0.1 n_{cr}, where n_{cr} is the critical electron density corresponding to each microwave frequency. For purposes of orientation, the above mentioned pulse widths and scalelengths roughly correspond to a Nd glass laser experiment with less than 50 psec duration and with a prepulse. The incident and backscattered electrogmagnetic waves are separated for detection using either a circulator or directional coupler, and then fed either into a square law detector for power measurements or into a spectrum analyzer for frequency shift measurements. The ion waves associated with SBS are detected using movable Langmuir probes. RF pick-up is not found to be a problem since the waves are measured long after the disappearance of the microwave pump. However, it should be noted that the ion frequency <u>during</u> the rf pulse may be considerably different than that measured afterwards since we are in the strong pump limit[3].

Convincing evidence for the existence of SBS in these microwave experiments is obtained by verifying that the energy and momentum selection rules, $\omega_o = \omega + \omega_s$ and $\underset{\sim}{k}_o = \underset{\sim}{k} + \underset{\sim}{k}_s$ are satisfied where $(\omega_o, \underset{\sim}{k}_o)$, $(\omega, \underset{\sim}{k})$, and $(\omega_s, \underset{\sim}{k}_s)$ are the frequency and wavenumber vector of the incident wave, ion wave, and scattered wave, respectively. In Fig. 1, the momentum selection rule is shown to be well satisfied for a variety of incident wavenumbers (k_o = 0.71, 1.15, 1.80 and 1.97 cm^{-1}) and ion species (He, Ne, Ar and Kr). The experimental value of k is determined from the wave phase velocity and frequency measured by an axially movable Langmuir probe. The solid line in Fig. 1 shows the relation $k = 2k_o'$, where k_o' is the wavenumber of the incident wave in the plasma ($k_o' \simeq 0.95\ k_o$ for $n_o \simeq 0.1\ n_{cr}$).

The verification of the SBS energy selection rule in microwave-plasma interactions is more difficult. Since τ_p is chosen to be small in order to avoid additional ionization of the background gas, the frequency shift between the incident and scattered waves is partially masked by the spectral broadening of the input microwave pulse itself. To measure the frequency shift of the reflected electromagnetic wave, we operated with the maximum ion wave frequency to provide the maximum frequency shift (390 kHz). The incident and reflected pulse spectra were obtained over many experimental pulses using a storage spectrum analyzer yielding a frequency shift of 210 kHz, with the shift in the red direction for the reflected wave. Considering that the reflected wave is a combination of the incident wave ($\tau_p \simeq 4\ \mu s$), unshifted reflected wave due to waveguide mismatches and chamber reflections, as well as the scattered wave, the agreement is close enough for us to feel that the energy selection rule is also satisfied in our experiment.

Figure 2 displays the scattered power P_s and the normalized density fluctuation level $(\tilde{n}/n_o)^2$ for experiments performed in an argon plasma using a

5.5 GHz microwave source. Since the microwave absorber material placed in the chamber to prevent reflections is not totally absorbing the residual reflected power without the plasma (≃ 2%) is subtracted from the total reflected power P_r to obtain P_s. Referring to Fig. 2, we observe that both P_s and $(\tilde{n}/n_o)^2$ initially increase exponentially and then begin to saturate with further increase of P_o. This saturation occurs when $\eta_\sigma = E_o^2/8\pi n_o KT_e \simeq 6$ and $v_o/v_e \simeq 0.9$, where $v_o = eE_o/m_e\omega_o$ is the quiver velocity of an electron in the field of the pump wave and $v_e = (KT_e/m_e)^{\frac{1}{2}}$. The corresponding values for 8.6 GHz are $\eta_o = 1.5$ and $v_o/v_e \simeq 0.45$. It should be noted that the density fluctuations displayed in Fig. 2(a) were measured quite far from the horn (≃ 60 cm) and are a factor of 2-3 lower than the peak fluctuations (see Fig. 3). We note that an almost linear relation between P_s and $(\tilde{n}/n_o)^2$ is obtained in the nonsaturated region.

The inset in Fig. 2(a) displays the time history of the incident microwave pulse (top) which rises to ≐ 70% maximum in ≤ 100 nsec together with the reflected microwave pulse (bottom) which grows and approaches steady state on the ion timescale. The initial fast rising portion of the reflected power trace is due to the residual chamber reflectivily as discussed above. Note the relatively smooth (nonspiky) nature of the reflected signal. The ion wave growth is seen to behave similarly as shown in the inset in Fig. 2(b) which displays $(\tilde{n}/n_o)$ obtained at a fixed time after turn-off of a variable duration 3.4 GHz rf pulse.

In Fig. 3, $\tilde{n}$ is shown as a function of axial distance from the horn. These data yield an interaction length ℓ for SBS, of about 94 cm (compare $\ell \simeq 130$ cm at 8.6 GHz). In this experiment, the interaction length appears to be limited in size by the divergence of the microwave beam; the measured density and temperature scale lengths are two and twenty times as large, respectively, as ℓ. We

therefore restrict ourselves to a discussion of SBS from a finite length homogeneous plasma.

For our parameters, the absolute instability threshold exceed the convective threshold by nearly an order of magnitude[1,3,6]. Therefore, finite interaction theory[1] yields the following convective threshold condition for SBS:

$$\int_0^{L_c} \left[\gamma_o^2(z)/c\gamma_s\right] dz = \frac{\gamma_o^2(o)\ell_t}{c\gamma_s} = 1 , \tag{1}$$

where

$$\gamma_o(z) = \frac{\sqrt{3}}{2}\left(k_o^2 v_o^2(z)\omega_{pi}^2/\omega_o\right)^{1/3} \tag{2}$$

is the spatially dependent strong coupling growth rate, γ_s is the damping rate of the ion wave, ω_{pi} is the ion plasma frequency and L_c is the chamber length.

The interaction length ℓ_t is calculated for several pumps in Table I. Here, P_{oth} is the threshold power obtained experimentally, A is the beam area, γ_o is calculated from Eq.(2)with (P_{oth}/A), and γ_s is obtained experimentally from the time history of the ion waves. We consistently find that $\ell \simeq \ell_t$ at the threshold value of pump power. In addition, we attempted to observe SBS for a pump wave of $\omega_o/2\pi = 16$ GHz and a power $P_o = 150$ kW. However, we did not observe the appropriate ion waves. For the above power level, the calculated value of $\ell_t \simeq 170$ cm $> \ell$. Thus, it also seems consistent that we could not find SBS as $\ell < \ell_t$ for this case.

When Eq.(1) is satisfied, the scattered power P_s arising from exponential growth out of the noise P_n is

$$P_s = P_n \exp(2\gamma_o^2\ell/\gamma_s c) , \tag{3}$$

where

$$P_n = \frac{P_o}{A} r_o^2 V_s^2 \tilde{n}_n^2 \Delta\Omega \qquad (4)$$

and $r_o^2 = 8 \times 10^{-26}$ cm^2, $V_s = A\ell$ is the scattering volume, A is the horn aperture cross section, R_o is the distance from the scattering center to the horn, $\Delta\Omega = A/R_o^2$ and $\tilde{n}_n$ is the background ion fluctuation level in the vicinity of $2k_o$. Figure 2 implies an exponential growth of P_s. This dependence on P_o is the same as predicted theoretically. Knowing the values of P_o, A, V_s, $\tilde{n}_n$ and $\Delta\Omega$ we can evaluate the backscattered power from Eqs.(3) and 4. The value of P_s estimated from this relation is in agreement with the experimentally measured value for all pump frequencies investigated. The threshold was also investigated by introducing a light ion mass impurity into the plasma. An increase appropriate to the increased Landau damping was observed.

Finally, let us consider the saturation mechanism(s). Phillion et al.[5] have suggested that ion heating could saturate SBS due to Landau damping of the ion waves. Following their expression, the ion heating rate can be estimated from the relation

$$\frac{d}{dt}(n_o K T_i) = \frac{P_o}{A\ell} r \frac{\omega}{\omega_o}, \qquad (5)$$

where ω/ω_o is the fraction of the reflected wave energy given to the ion waves and r is the reflectivity. When the present experimental Parameters are inserted, we require a pulse width of $\tau_p > 5 \times 10^{-5}$ sec to observe the appropriate ion heating. Energy analyzer measurements have verified the lack of ion main body heating for the present pulse durations.

Kruer[7] has proposed that the backscatter can be limited by a saturation of the ion waves due to trapping. Using a water-bag model for the ions he predicts that $(\tilde{n}/n_o)_{max}$ is given by

$$\left(\frac{\tilde{n}}{n_o}\right)_{max} = \frac{1}{2}\left\{ \left[1 + \frac{T_i}{T_e}\right]^{\frac{1}{2}} - \left[3T_i/T_e\right]^{\frac{1}{2}} \right\}^2 \qquad (6)$$

which yields $\left(\frac{\tilde{n}}{n_o}\right)_{max} \simeq 13\%$ for $T_e/T_i \simeq 10\text{-}12$. This value $(\tilde{n}/n_o)_{max}$ is approximately a factor of two to three times larger than our observed $\tilde{n}/n_o = 5\%$.

Finally, Ikezi et al.[8] have observed both experimentally and numerically nonlinear frequency or wavenumber shifts in ion acoustic waves which are attributed to trapped ions. This shift can limit SBS to densities below that given by Eq. (6) by moving the ion frequency out of the resonance region which is quite narrow ($\simeq 8\%$) for our parameters. Using their Eq. (28) obtained from a kinetic treatment of the ions we estimate a limiting density fluctuation level $\tilde{n}/n_o \simeq 3.5\%$ which is in excellent agreement with our observed value. It should be noted that energy analyzer measurements indicate the presence of a population of accelerated ions traveling at $\simeq 2\ c_s$ produced by the rf pulse.

In conclusion, we have observed, for the first time, stimulated Brillouin scattering in a microwave-plasma interaction. The results obtained in our experiment are consistent with the theory for a finite homogeneous plasma. Saturation of the scattered wave is observed which is consistent with ion trapping.

We would like to thank Drs. J. J. Thomson, J. Kindel, W. Kruer, D. Forslund, K. Estabrook, J. Dawson, B. Ripin and M. Herbst for helpful conversations concerning the saturation processes for SBS. This work was supported in part by the Office of Laser Fusion, U. S. Department of Energy, Contract No. DE-AS03-76-SF00034, PA DE-AT03-76DP40010, and U. S. Air Force Office of Scientific Research Contract No. F49620-76-C-0012.

REFERENCES

1. D. Pesme, G. Laval, and E. Pellat, Phys. Rev. Lett. 31. 203 (1973).

2. C. S. Liu, M. N. Rosenbluth and R. B. White, Phys. Fluids 17, 1211 (1974).

3. D. W. Forslund, J. M. Kindel and E. L. Lindman, Phys. Fluids 18, 1002 and 1017 (1975), and references therein.

4. B. H. Ripin, F. C. Young, J. A. Stamper, C. M. Armstrong, R. Decoste, E. McLean and S. E. Bodner, Phys. Rev. Lett. 29, 611 (1977).

5. D. W. Phillion, W. L. Kruer and V. C. Rupert, Phys. Rev. Lett. 39, 1529 (1977).

6. W. M. Manheimer, Phys. Fluids 17, 1634 (1974).

7. W. L. Kruer, UCRL Preprint 82701, to be published (1979). Also, J. M. Dawson, W. L. Kruer and B. Rosen, in Dynamics of Ionized Gases, edited by M. Lighthill, I. Imai and H. Sato, (Univ. of Tokyo Press, Tokyo, 1973) pg. 47-61.

8. H. Ikezi, K. Schwarzenegger, A. L. Simons, Y. Ohsawa and T. Kamimura, Phys. Fluids 21, 247 (1978).

f_o (GHz)	τ_p (μsec)	$I(o)=P_{oth}/A$ (W/cm^2)	$\gamma_o(o)$ (sec^{-1})	γ_s (sec^{-1})	ℓ_t (cm)
3.4	3	645	3.2×10^6	2.5×10^4	73
5.5	4	987	4.3×10^6	4.0×10^4	65
8.6	5	564	4.2×10^6	5.0×10^4	85

Table 1. Calculated value of threshold interaction length for several pump frequencies.

FIGURE CAPTIONS

Fig. 1 Wavenumber of ion waves versus incident electromagnetic wavenumber.

Fig. 2(a) Ion wave amplitude (z = 60cm) versus incident power (τ_p = 4 μsec).

Fig. 2(b) Scattered power versus incident power (τ_p = 4 μsec).

Fig. 3 Spatial variation of density fluctuation amplitude (τ_p = 4 μsec).

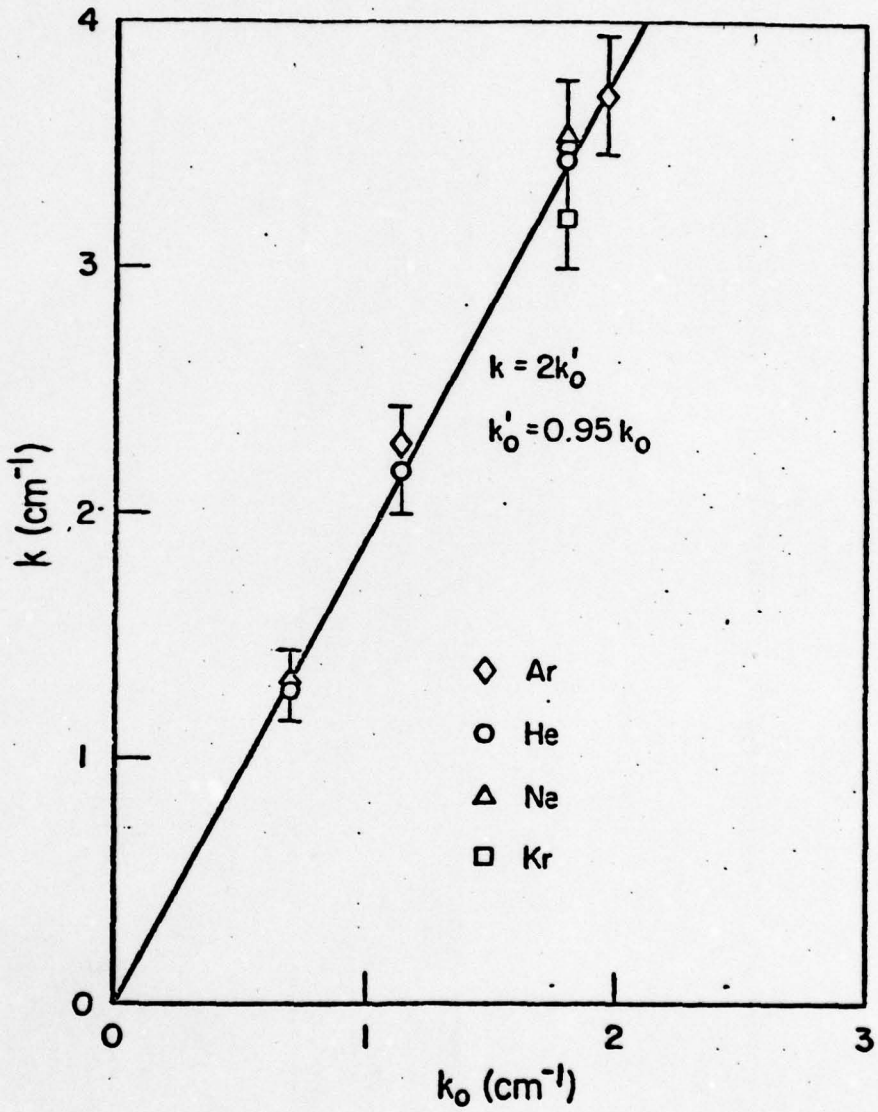

Fig. 1 Wavenumber of ion waves versus incident electromagnetic wavenumber.

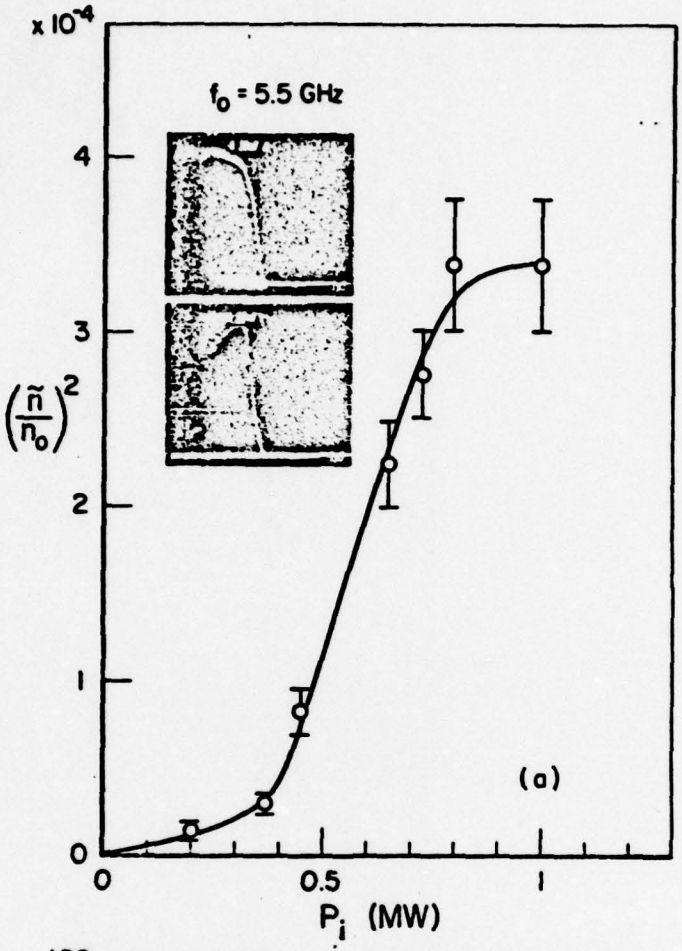

Ion wave amplitude (Z = 60cm) versus incident power(τ_p=4 μs

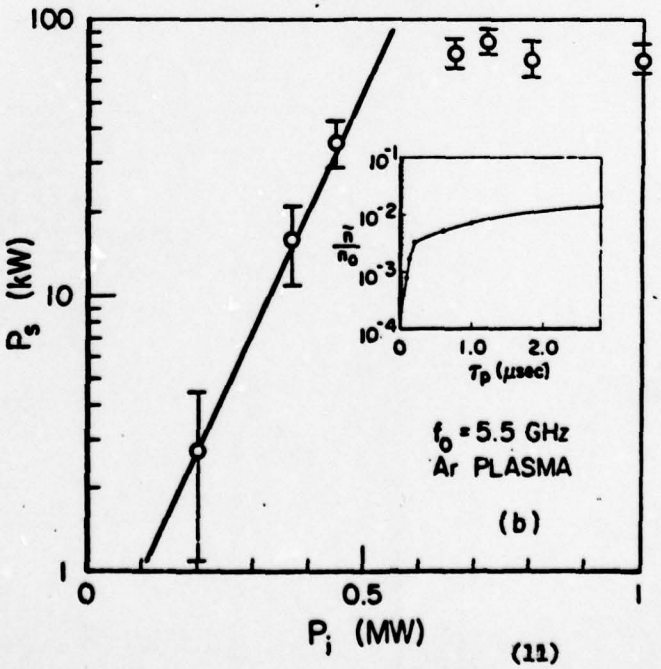

Scattered power versus incident power (τ_p= 4 μsec)

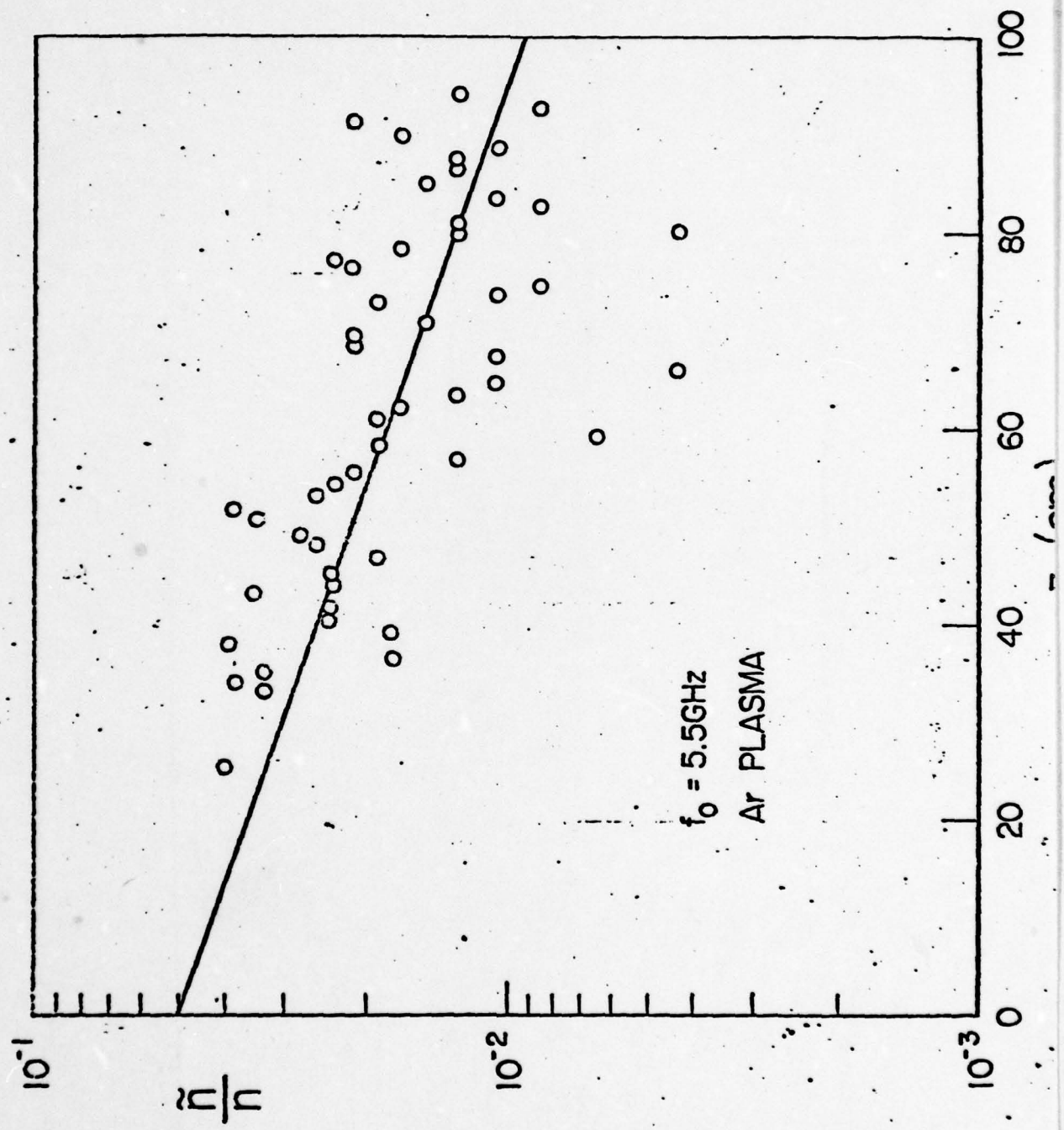

Fig. 3 Spatial variation of density fluctuation amplitude (τ_p = 4 μsec).

APPENDIX II

OBSERVATION OF THE SOLITON FLASH

M. Rhodes, Ann Lee, Y. Nishida,
N. C. Luhmann, Jr., and S. P. Obenschain

PPG-428 September 1979

Electrical Sciences & Engineering Department
University of California
Los Angeles, California 90024

noted that the ion frequency during the rf pulse may be considerably different than that measured afterwards since we are in the strong pump limit[3].

OBSERVATION OF THE SOLITON FLASH

M. Rhodes, Ann Lee, Y. Nishida*, N. C. Luhmann, Jr., and S. P. Obenschain**

University of California, Los Angeles, CA 90024

The soliton flash is observed in an unmagnetized inhomogeneous laboratory plasma. The Langmuir wave energy is observed to narrow spatially and to rapidly grow to its peak value at $\omega_{pi}\,\tau \simeq 24$ and then collapse. Coincident with this flash are increased hot electron production ($\varepsilon_h > 10\,\varepsilon_e$), a large increase in the ion wave energy and the maximum growth rate of the spontaneous magnetic field.

*Permanent Address: Faculty of Engineering
Utsunomiya University
Utsunomiya, Japan

** Permanent Address: Naval Research Laboratory
Washington, D.C.

The absorption of electromagnetic energy in the vicinity of the critical layer ($\omega_o \simeq \omega_p(x_c)$ is of importance both to laser pellet fusion and rf heating of magnetically confined plasmas. In laser fusion, much attention has been given to the process of resonance absorption.[1-4] Here, an electromagnetic wave, obliquely incident to the plasma density gradient, is partially reflected at the cutoff layer $\omega_o \simeq \omega_p (x_{co})/\cos\theta$, and tunnels to the critical layer where the parallel component of the electric field generates Langmuir waves, which in turn deposit their energy as they propagate down the density gradient. In addition, the ponderomotive force due to the spatially localized field can expel plasma leading to a density cavity and associated density streamers.[5] Numerical solutions of the mode-coupling equations applied to the resonance absorption problem predict that the Langmuir soliton, after growing to large amplitude, suddenly decreases in amplitude at $\omega_{pi}\,\tau \simeq 13$. This process has been referred to as "Soliton Flash."[5,6] Associated with the decrease in the Langmuir wave energy is a concomitant increase in ion acoustic wave energy. After the flash, the pump energy is converted directly into ion waves. Since such processes as spontaneous magnetic field generation,[7] hot electron production, and return current driven ion acoustic instabilities[8] depend sensitively on the details of resonance absorption, it is of importance to experimentally examine the specific predictions of the Soliton Flash theory.

Herein we present results on the observation of the soliton flash and its relation to the above mentioned phenomena. The experiments were performed in a cylindrical unmagnetized plasma (60 cm diam, 80 cm length) produced by a multi-filament discharge. Pulsed microwave radiation ($f_o = (\omega_o/2\pi) \simeq$ 3GHz) of typical risetime $\tau_o \simeq 10$ nsec is launched from a gridded horn (aperture $\simeq 2\ \lambda_o$) along the z-axis. The plasma density increases along z ($n|dn/dz|^{-1} \simeq 50$ cm $\simeq 5\ \lambda_o$). There is also a relatively gentle density gradient parallel to the main component of the incident electric field E_x ($n|dn/dx|^{-1} \simeq 200$ cm). Typical plasma parameters are $n_e \simeq 10^{11}$ cm^{-3}, $T_e \simeq 2.5$ eV, $T_e/T_i \simeq 10$, $n_n \simeq 10^{13}$ cm^{-3} and electron collision frequency $\nu/\omega_o \simeq 10^{-5}$. The calculated value of $\eta_{vac} = E_{vac}^2/8\pi nKT_e$ is approximately 1% at an incident power of 2.4 kW, where E_{vac} is the vacuum field strength. This is approximately the external energy density employed in the calculations of Ref. 5 and 6 and the highest power utilized in the present experiments.

The soliton flash is clearly evident in Fig. 1 which displays the time evolution of the high frequency electric field intensity in the vicinity of the critical layer. The result of Elsässer and Schamel[6] is also shown for comparison purposes. As can be seen from Fig. 1(a), the electric field intensity initially grows gradually in amplitude, and at $\omega_{pi}\ \tau \simeq 24$ abruptly decreases as predicted theoretically. The flash time, as well as the detailed shape of the electric field curve [see Fig. 1(b)], are in

reasonable agreement (factor of 2) with the prediction of Elsässer and Schamel ($\omega_{pi}\,\tau \simeq 13$). Furthermore, we investigated the scaling of the flash time with ion mass for a variety of ion species (H, He, Ne, Ar and Kr) and found it to vary as $m^{1/2}$ as predicted theoretically. In addition, the flash time τ was found to be weakly dependent on incident power once the threshold field strength $\eta_{vac} = 0.05\%$ was exceeded ($\tau \propto P^{-0.2}$).

In Fig. 2 are shown the temporal evolution of the axial distribution of the electric field intensity and the density cavity. The position of the resonance layer was identified both by a determination of the source region for the density streamers observed to propagate up and down the density gradient [5], and also by a measurement of the axial electric field profile at low power which clearly showed the cutoff and resonant layers. As can be seen from Fig. 2(a), the electric field initially both narrows spatially and grows in amplitude. After the flash, the high frequency field energy abruptly decreases even if the microwave pump field is maintained at constant amplitude, as is predicted by theory.[6] In Fig. 2(b) is shown the evolution of the density cavity. At the soliton flash, the development of a large density cavity occurs in the same region where the field intensity maximizes. Using our measured values of the streamer extrema and the temporal width of the field collapse, we find the observed half width of the soliton ($\Delta x \simeq 2$ cm) to be in good agreement with the predictions of Elsässer and Schamel.[6]

Coincident with the Soliton Flash, a large burst of hot electrons ($\varepsilon > 10\varepsilon_e$) is observed with both a retarding grid energy analyzer (see Fig. 3) and a Langmuir probe where ε_e is the electron thermal energy. After the collapse, the hot electron current decreases to approximately 15% of its peak value. This is to be expected from the numerical solutions[5,6] where η exceeds unity at the time of collapse even for an initial $\eta_{vac} \leq 10^{-2}$. Therefore, the wave-breaking amplitude[9,10] is reached for the resonantly driven electron waves and strong hot electron production is observed.

The electric field strength may be estimated by several methods. First, from the measured hot electron energy, the wave breaking velocity v_{br} is obtained yielding $E_{br} = v_{br} m\omega_o/e \simeq 2.8$kV/cm. Second, from Ref. 10

$$v_{br} = 1.2\, v_d (\omega_o L/v_e)^{2/3} \qquad (1)$$

where $v_d = eE_d/m\omega_o$, v_e is the electron thermal velocity and L is the density scale length. Using our parameters Eq. (1) yields $v_{br} \simeq 3 \times 10^8$cm/sec or $E_{br} \simeq 2.4$kV/cm. The high frequency electric field may also be estimated from the maximum amplitude of the ion wave streamer, $\delta n_{max}/n$, using the relation[5]

$$W^2 = \frac{|E|^2}{4\pi n_o K, T_e} = \frac{1}{0.76} \frac{\delta n_{max}}{n} \frac{1+\beta^2}{\beta} \qquad (2)$$

where $\beta = Z_o/c_s\tau_o$ with Z_o the width of the soliton and τ_o the temporal width of the collapse. Using our measured values of Z_o, τ_o and $\delta n_{max}/n$, $W^2 = 2.2$ (i.e. $E_z = 1.1$kV/cm) is obtained which is in reasonable agreement with the above mentioned hot electron measurements.

The spatial and temporal dependence of the quasi-static magnetic field produced by resonance absorption[11,12] was investigated and found to be closely related to the soliton flash. As shown in Fig. 3, the maximum growth rate of the magnetic field for $\omega_{pi}t \leq 100$ is found to coincide with the soliton flash time regardless of spatial position. This coincidence seems consistent since as discussed earlier, the soliton flash induces hot electron emission due to wave breaking, and the associated currents can produce the observed magnetic fields.

The electron distribution function was investigated in considerable detail. It was found that the hot electron region has an abrupt cutoff and that the high energy tail has two temperatures, with the lower energy portion comprising approximately 2.5% of the total electron population while the higher energy region contains 1% of the electrons. These hot electrons are mainly emitted toward the underdense plasma. The break point between the two regions ΔE is found to scale with incident rf power as $P^{0.85}$ for $P < 500W$ ($\eta < 2\times10^{-3}$) and to be relatively independent of power for $P > 500W$ [see Fig. 4(a)]. The temperature of the lower energy region increases as $P^{0.72}$ as also shown in Fig. 4(a), while that of the higher energy region increases as $P^{0.32}$. It is instructive to compare these results with the models of Forslund et al.[13] and Albritton et al.[14] They appear to predict only a single hot electron temperature which for lower intensities scales as $T_H \propto P^{0.67}$ while for higher intensities $T_H \propto P^{0.25}$. Therefore, the two temperature hot electron distribution

appears to require further theoretical explanation. The calculated hot electron density is ≃ 4%, using Eq. (6) from Ref. 14, which is in reasonable agreement with the experimental results. It should be noted that similar hot electron distributions have been observed in other microwave simulation experiments.[15]

The ion wave energy was investigated as a function of time. This was done by varying the width of the incident microwave pulse and monitoring the peak to peak amplitude of the ion wave streamers at a fixed spatial position and time after rf turn-off (≃ 20μsec). The choice of measurement time is not critical due to the weak wave damping. An example of the data is shown in Fig. 4(b). As can be seen in Fig. 4(b), the ion wave energy increases exponentially until the Soliton Flash occurs and then becomes relatively constant for further increase in pulse duration. The initial growth time is about 40nsec ($\gtrsim \omega_{pi}^{-1}$) in this example. These results are in agreement with the numerical calculations of Ref. 6. The streamer amplitude $\delta n/n$ is found to scale with rf power as $P^{0.8}$ for $\eta_{vac} \lesssim 2 \times 10^{-3}$ while the flash peak electric field intensity E^2 scales as $P^{1.8}$. Referring to Eq. (2) we see that the above implies that $\beta \propto P^{1.0}$ since $\beta \simeq 20$ for our parameters. For $2 \times 10^{-3} < \eta_{vac} \lesssim 10^{-2}$, the streamer amplitude is essentially constant and strong high frequency turbulence ($f \gtrsim f_{pe}$) is observed, with E^2 now scaling as $P^{1.0}$.

In addition to the above mentioned low frequency ion wave streamers, we observe high frequency ($\omega/\omega_{pi} \simeq 0.14$) relatively coherent ion waves possibly due to cold electron return current driven instabilities. These

exist both in the region $\lambda_o/2$ below the critical layer (essentially, between the resonance and cutoff layers) and the region slightly above critical ($\simeq 0.1 \sim 0.2\lambda_o$). For $\eta_{vac} \lesssim 3 \times 10^{-4}$, $\delta n/n \propto P^{1.0}$ for these waves. For $\eta_{vac} \gtrsim 3 \times 10^{-4}$ (in the region where the solition flash sets in) $\delta n/n$ is relatively independent of the power and higher frequency modes start.

That the soliton flash occurs at the cutoff, not the resonance layer, was investigated in detail. The high frequency electric field energy is found to propagate both up and down the density gradient after the Soliton Flash. The upstream energy, or wave packet, with a velocity of $\simeq 0.05 \sim 0.1V_e$, reaches the resonance layer where it disappears and simultaneously ion wave streamers are observed to be emitted from the resonance layer. The down streaming packet has a velocity of $V_e/3$, and disappears within a few centimeters.

In conclusion, we have observed behavior in agreement with the Soliton Flash theory[5,6]. It should be noted that some of the features described here, such as the initial rapid growth and subsequent decay of the high frequency field, have been observed previously in a simple capacitor plate geometry[16]. However, since the source and detector responsivity were limited to $\omega_{pi}t \simeq 4$[16] the authors were unable to make the detailed comparison with theory described herein. Furthermore, herein the Soliton Flash was found to be correlated with such phenomena as spontaneous magnetic field generation and hot electron production. The channeling of rf energy into ion waves observed in the present experiment appears to be of particular relevance to the process of energy absorption in laser pellet fusion.

ACKNOWLEDGEMENTS

We would like to thank G. Huffman of Varian Associates and J. Quinn of EIMAC for their generous assistance which made these studies possible. This work was supported in part by the Office of Laser Fusion, U. S. Department of Energy, Contract No. DE-AS03-SF00034, PA DE-AT03-76 DP40010 and U. S. Air Force Office of Scientific Research, Contract No. F49620-76-C-0012.

REFERENCES

1. W. L. Kruer, R. A. Haas, W. C. Mead, D. W. Phillon and V. C. Rupert, in Plasma Physics (Plenum Publishing Corp., New York) 1977.

2. C. E. Max, Bull. Am. Phys. Soc. 1977.

3. T. Speziale and P. J. Catto, Phys. Fluids 20, 990 (1977).

4. D. W. Forslund, J. M. Kindel, K. Lee, E. L. Lindman and R. L. Morse, Phys. Rev. Ali, 679 (1975).

5. H. Schamel and K. Elsässer, Plasma Physics 20, 837 (1978).

6. K. Elsässer and H. Schamel, Plasma Physics 19, 1055 (1977).

7. C. E. Max, W. M. Manheimer andJ. J. Thomson, Phys. Fluids 21, 128 (1978).

8. W. Manheimer and D. G. Colombant, Phys. Fluids 21, 1818 (1978).

9. K. G. Estabrook, E. J. Valeo and W. L. Kruer, Phys. Fluids 18, 1151 (1975).

10. W. L. Kruer, Phys. Fluids 22, 1111 (1979).

11. W. F. DiVergilio, A. Y. Wong, H. C. Kim and Y. C. Lee, Phys, Rev. Lett. 38, 541 (1977).

12. S. P. Obenschain and N. C. Luhmann, Jr., Phys. Rev. Lett. 42, 311 (1979).

13. D. W. Forslund, J. M. Kindel and K. Lee, Phys. Rev. Lett. 39, 284 (1977).

14. J. R. Albritton, E. I. Thorsos, and E. A. Williams, (private communication, to be published) 1978.

15. W. F. DiVergilio, (private communication) 1979.

16. A. Y. Wong, in Laser Interaction and Related Plasma Phenomena, Vol. 4B, edited by H. J. Schwarz and H. Hora (Phenum Press, New York) 1977 and references therein.

FIGURE CAPTIONS

Fig. 1(a) Electric field intensity, E^2, as a function of time. Upper trace shows the microwave pulse shape (pulse width is 5μs).

(b) Numerical result after Ref. 6.

Fig. 2 The evolution of the axial distribution of (a) the electric field, and (b) the density cavity. The resonance layer is at 30 cm.

Fig. 3 Time dependence of the hot electron current ($\varepsilon > 10\ \varepsilon_e$), high frequency electric field intensity $|E|^2$, largest component of the spontaneous magnetic field and its derivative together with rf input pulse.

Fig. 4(a) Hot electron temperature, T_{hot}, in the lower energy region and energy of the break-point, ΔE, as a function of incident power. Solid lines are least square fits to the data using the points below 500W.

Fig. 4(b) Ion wave streamer amplitude vs. rf pulse duration. The inset is a typical example of the ion wave streamer observed in the overdense region.

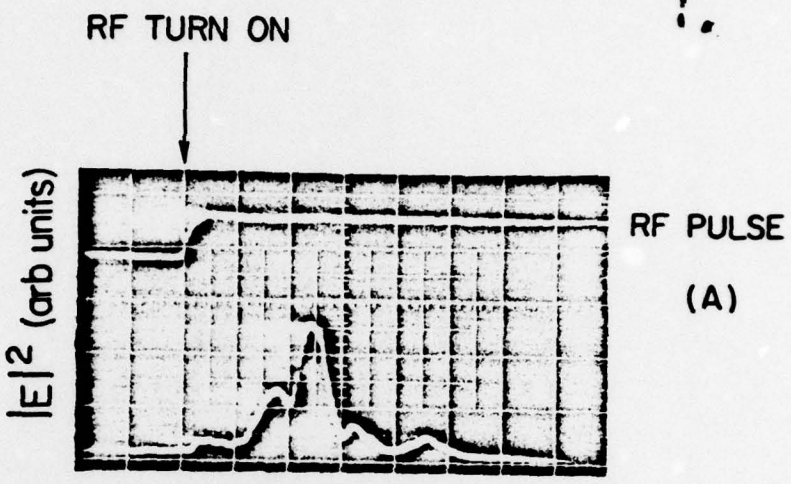
RF TURN ON
$|E|^2$ (arb units)
RF PULSE
(A)

200 ns/div

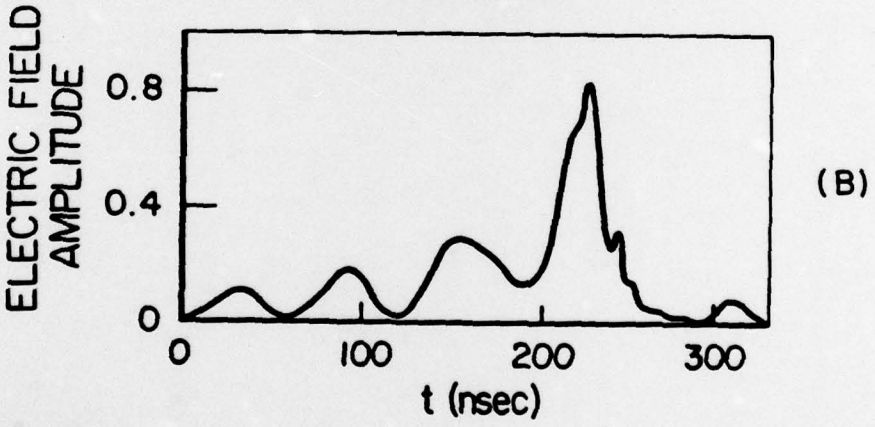
ELECTRIC FIELD AMPLITUDE
0.8
0.4
0
0
100
200
300
t (nsec)
(B)

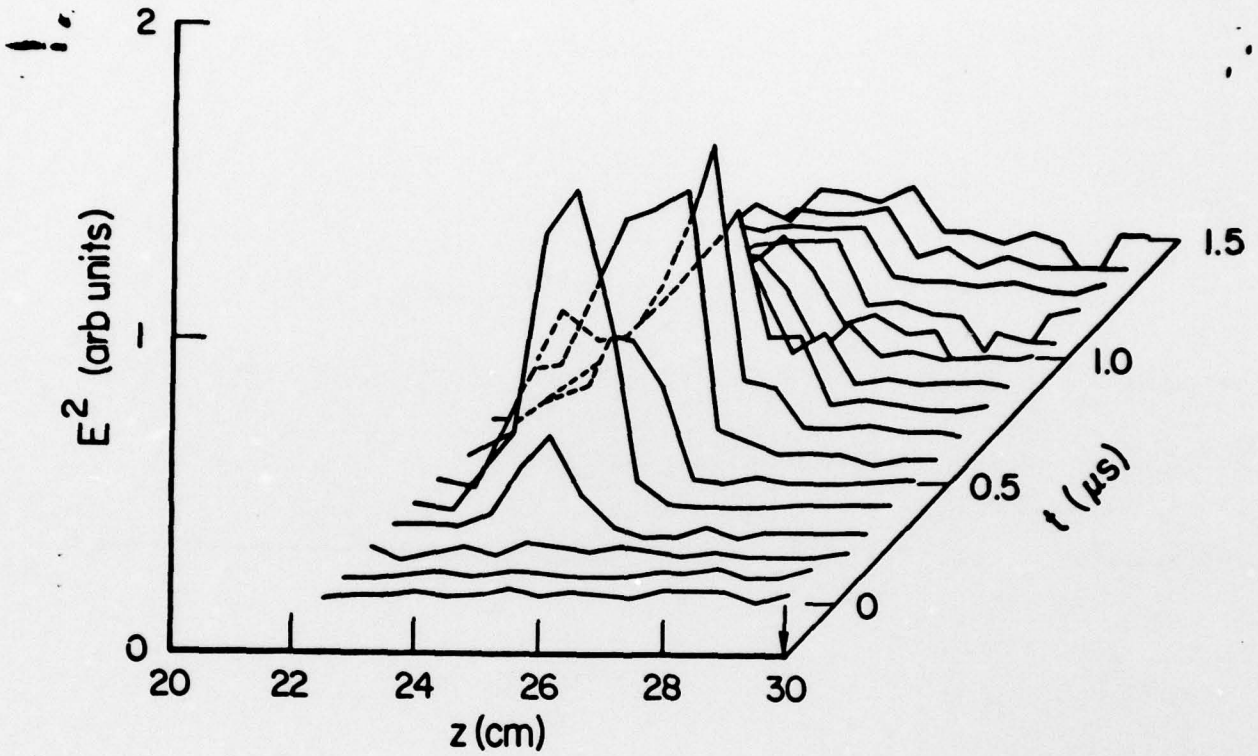
2
1
0
E^2 (arb units)
20
22
24
26
28
30
z (cm)
0
0.5
1.0
1.5
t (μs)

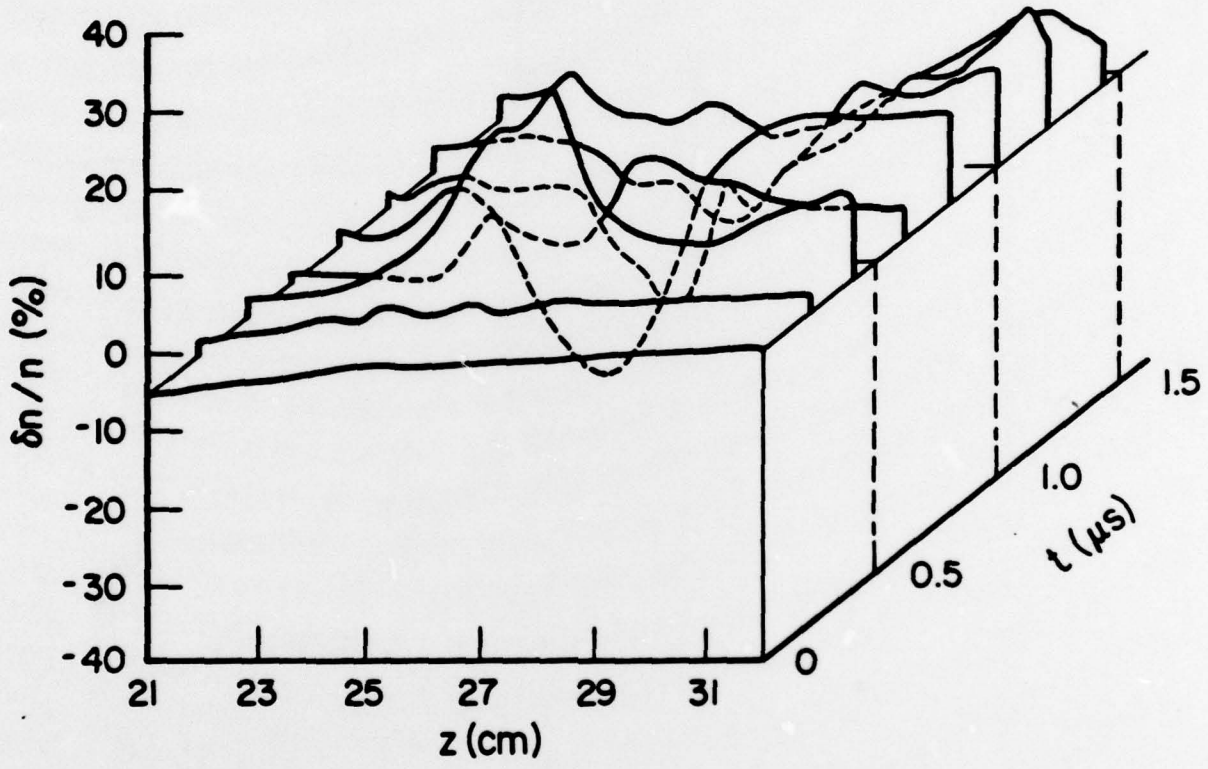
40
30
20
10
0
-10
-20
-30
-40
δn/n (%)
21
23
25
27
29
31
z (cm)
0
0.5
1.0
1.5
t (μs)

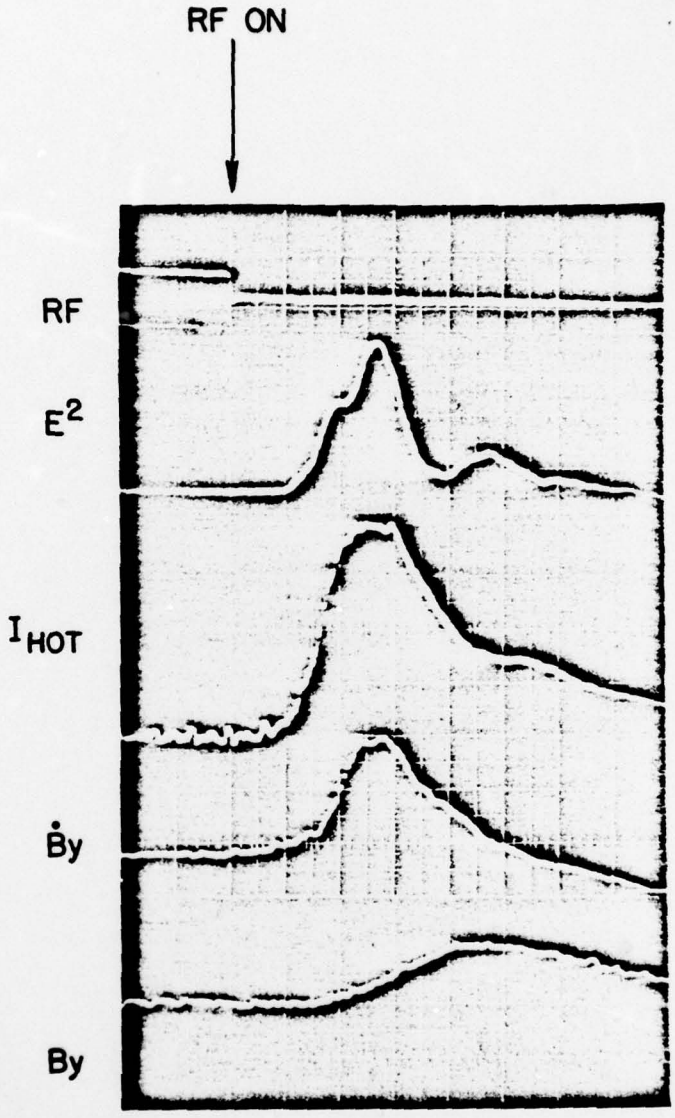
RF ON
RF
E^2
I_{HOT}
$\dot{B}y$
By
200 n sec/div

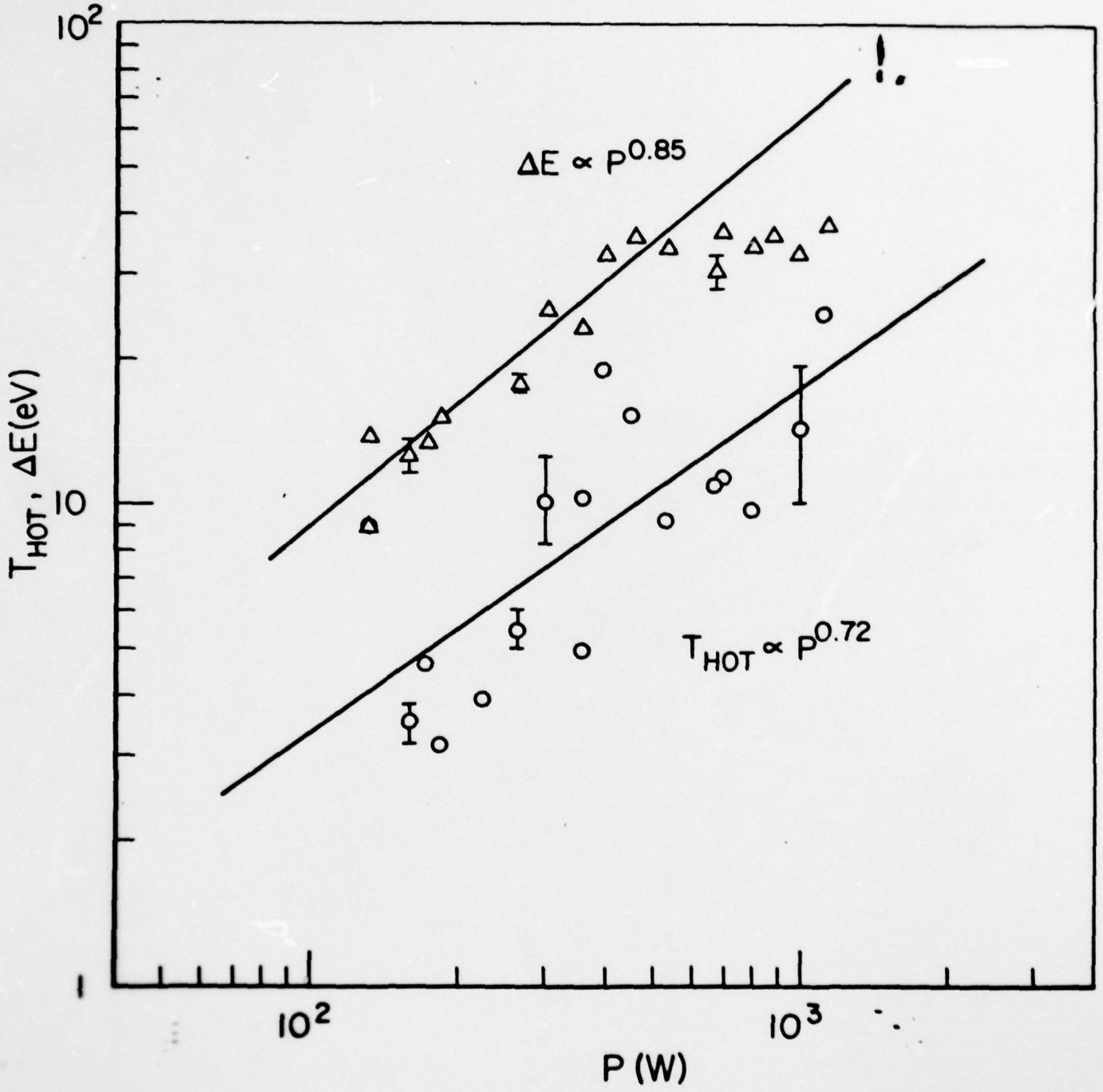
10^2
10
1
T_{HOT}, ΔE(eV)
$\Delta E \propto P^{0.85}$
$T_{HOT} \propto P^{0.72}$
10^2
10^3
P (W)

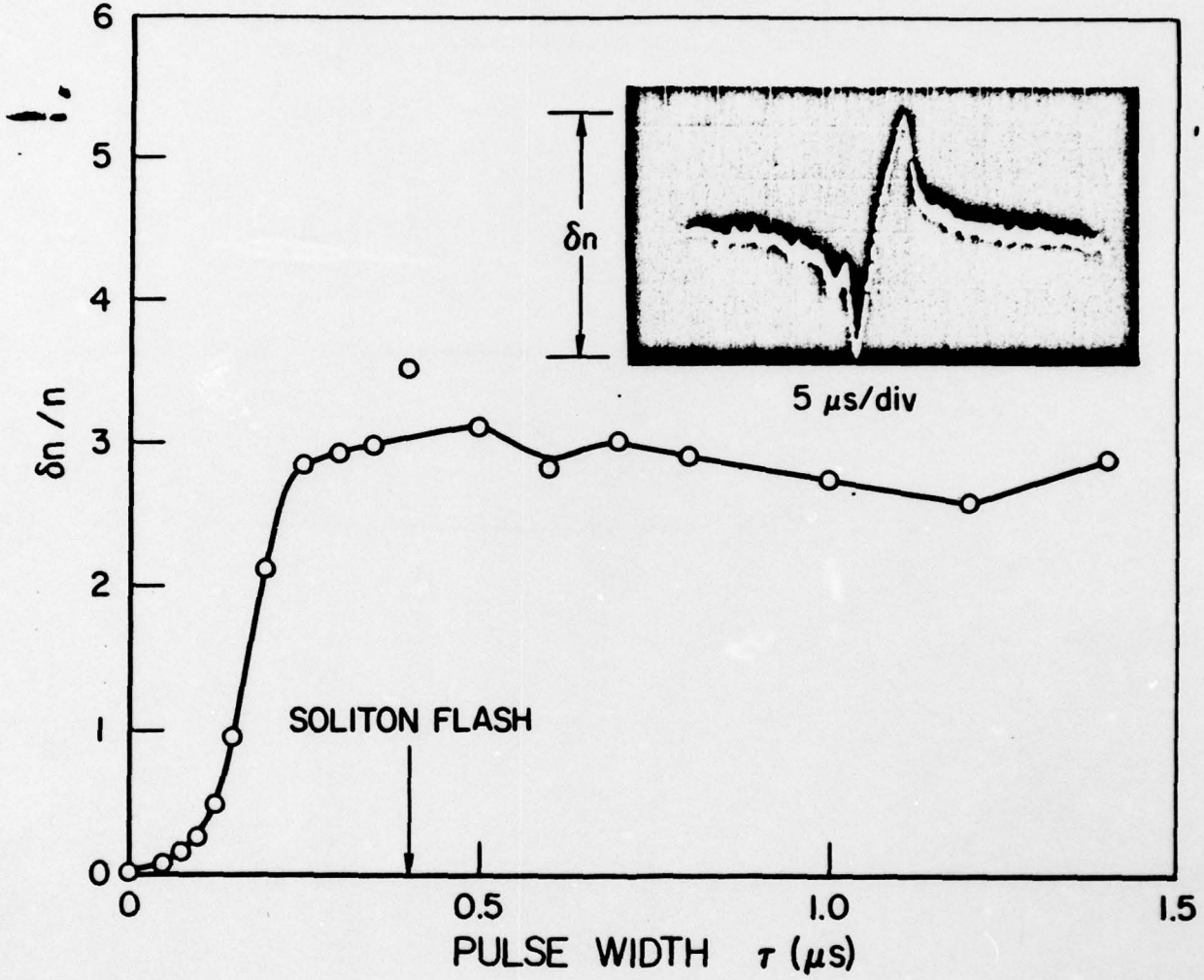
6
5
4
3
2
1
0
δn/n
δn
5 μs/div
SOLITON FLASH
0
0.5
1.0
1.5
PULSE WIDTH τ (μs)